1-1-1983

Failure prediction based on strain energy density criterion for crack and notch problems in thermoelasticity.

Robert Charles Bolton

FAILURE PREDICTION BASED ON STRAIN ENERGY DENSITY CRITERION FOR CRACK AND NOTCH PROBLEMS IN THERMOELASTICITY

by

Robert Charles Bolton

A Thesis

Presented to the Graduate Committee

of Lehigh University

in Candidacy for the Degree of

Master of Science

in

Applied Mechanics

Lehigh University

1983

This thesis is accepted and approved in partial fulfillment of the requirements for the degree of Master of Science.

Sept. 14, 1983
(date)

Professor in Charge

Chairman of Department

ACKNOWLEDGEMENTS

The author would like to thank Professor G. C. Sih for the seed from which this thesis was developed; his fellow graduate students with the Institute of Fracture and Solid Mechanics for their input; Barbara DeLazaro for her invaluable assistance in the final preparation of this thesis; and his wife, Lynne, for her unfailing encouragement and support.

TABLE OF CONTENTS

LIST OF TABLES

LIST OF TABLES - (Continued)

LIST OF FIGURES

LIST OF FIGURES - (Continued)

LIST OF FIGURES - (continued)

ABSTRACT

The strain energy density failure criterion is applied to steady-state, uncoupled, thermoelastic problems involving cracks and notches in domains with finite boundaries. In contrast to classical fracture mechanics theory, the strain energy density criterion can be used to predict both the origin of failure on the notch and crack trajectories for non-isothermal problems where the crack paths are generally curved. The problems are solved numerically for a variety of boundary conditions using the finite element method. Both thermal and combined thermal and mechanical loadings are considered. The validity of the numerical method is established by comparing the numerical solution of a narrow notch in an uniform heat flow to the corresponding analytical solution for a line crack.

The numerical results are presented in both graphic and tabular form. The proportion of mechanical to thermal loading is shown to affect the predicted fracture trajectories. Increasing mechanical loading shifts the trajectories toward the plane of symmetry of the mechanical loading. The effect of notch sharpness is examined by varying the ratio of the minor to major axes of the elliptical notches. Narrowing the notch primarily increases the intensity of the strain energy density field close to the notch tip. The effect of the form of the strain energy density function (dW/dV) is considered. When expressed in terms of the strain component, dW/dV contains a term, C_o, which is commonly neglected. It is shown that this term is a

function of temperature and the material properties and hence, cannot be neglected in non-isothermal cases. Omission of this term is shown to give incorrect, and often, non-physical results for dW/dV and for crack trajectory prediction.

I. INTRODUCTION

Geometric discontinuities such as re-entrant corners, notches, cracks and other defects can result in local stresses many times higher than those at distances further away. These localized stress concentrations can have a significant influence on the load bearing capacity of structural components. The stress analyses of such problems are not always straightforward as they require a great deal of accuracy near locations where the stress gradients are high. In particular, numerical inaccuracies in stress analysis can directly influence the life prediction of components that are an essential consideration in design.

A prerequisite in finding allowable loads and net section size of structural components is to have a reliable failure criterion. The classical theory of fracture mechanics, although accounting for the influence of initial defects, cannot adequately treat problems where the crack path tends to curve. This is basically because the concept of energy release rate or critical stress intensity factor is limited to self-similar crack growth where the crack runs in a straight path. This shortcoming has been circumvented by the strain energy density criterion of Sih [1]. This is particularly important in non-isothermal problems because cracks will turn as a rule rather than the exception. A case in point is that of an insulated crack engulfed by uniform heat flow. The temperature field acquires different signs across the crack plane. Failure behavior of non-isothermal solids

obviously depends on the energy level at which they are subjected to. Hence, any criterion based on stress or strain alone would have to be seriously questioned. Particular attention must, therefore, be focused on calculating the energy state when performing failure analysis. This has been pointed out in [2] with regard to the determination of the strain energy density function in thermal elasticity.

Since failure tends to initiate from locations of severe change in geometry, it is pertinent to have a quantitative assessment of this severity. A mathematically sharp crack with zero radius of curvature, for example, can behave differently from that with a finite curvature. This influence has been studied in detail for the isothermal case [3, 4] of an elliptical opening which, in the limit, reduces to a sharp crack. The predicted crack trajectories near the ends of the ellipse differed considerably from those near the crack tips. A further study of the notch effect is carried out in this thesis when the temperature can vary from point to point in the solid.

Considered in this work is the finite element formulation of thermoelastic problems with cracks. The strain energy density criterion is applied to forecast crack trajectories for several problems involving non-uniform temperature distribution. Mechanical loading effects are also discussed with regard to their interaction with the thermally induced stresses. The numerical results are displayed graphically and agreed well with those obtained analytically for the problem of heat flow passing an insulated crack.

II. STRAIN ENERGY DENSITY CRITERION

The strain energy density criterion [1,5] predicts failure by yielding and/or fracture on the basis that the stationary values of the strain energy density function dW/dV can be identified with the sites of material damage. The approach involves calculating the stored energy in an element of material located at a finite distance, say r_o, ahead of the crack. The location of relative minimum of dW/dV or $(dW/dV)_{min}$ is assumed to coincide with that of incipient fracture while the relative maximum $(dW/dV)_{max}$ with that of incipient yielding. Their critical values depend on the material.

Without loss in generality, dW/dV may be expressed in the form

$$\frac{dW}{dV} = \frac{S}{r} \tag{1}$$

in which S is known as the strain energy density factor and r is a linear distance measured from the point of failure initiation site. Only in the case of linear elasticity, dW/dV may be regarded as the sum of two components, say, denoted by $(dW/dV)_v$ and $(dW/dV)_d$. The former refers to dilatation and the latter to distortion. It can be shown that $(dW/dV)_v > (dW/dV)_d$ holds at sites predicted to failure by fracture and $(dW/dV)_v < (dW/dV)_d$ at sites that undergo yielding. No such interpretation prevails when the influence of plasticity becomes significant.

In what follows, only the onset of fracture will be treated. Hence, it suffices to consider $(dW/dV)_{min}$ reaching a critical value, say, $(dW/dV)_c$, which corresponds to the area under the true stress and strain curve. For a linear elastic material, tested to failure under uniaxial loading and isothermal condition, $(dW/dV)_c$ is simply equal to $\sigma_{yd}^2/2E$ where σ_{yd} is the yield strength and E the Young's modulus. The critical value S_c can, of course, be computed from $(dW/dV)_c$ and r_c in accordance with equation (1).

The basic assumptions of the strain energy density criterion [1, 5] can thus be summarized as follows:

(1) Fracture initiation sites are assumed to coincide with locations of relative minima of dW/dV or $(dW/dV)_{min}$.

(2) Fracture initiation is assumed to occur when $(dW/dV)_{min}$ reaches a critical value $(dW/dV)_c$ being characteristic of the material.

When the crack growth occurs, additional conditions are required to describe the rate at which is being damaged. This, however, is beyond the scope of this work. Refer to [5] for details.

A. STRAIN ENERGY DENSITY FUNCTION IN THERMAL ELASTICITY

Caution should be exercised in applying the strain energy density criterion to thermal elastic problems where the temperature gradients prevail throughout the solid. In particular, dW/dV is dependent not

only on the state of stress and strain but the level of thermal energy. The latter contribution has been overlooked [6] when formulating thermal elasticity by expanding dW/dV in terms of the strain components e_{ij}:

$$(C_o + C_{ij}e_{ij} + C_{ijk\ell}e_{ij}e_{k\ell} + \ldots) \tag{2}$$

The coefficient C_o is associated with the energy density of the reference state and was neglected in [6]. Let the temperature at a given point in the solid be $T(x,y,z)$ and T_o be a constant reference temperature. The expression for dW/dV in linear thermal elasticity is [7]

$$\frac{dW}{dV} = \frac{1}{2}\sigma_{ij}e_{ij} - \frac{1}{2}\alpha(T-T_o)\sigma_{kk} \tag{3}$$

where α is the coefficient of thermal expansion and σ_{kk} is the first stress invariant. Making use of the linear isotropic forms of the stress-strain relation

$$\sigma_{ij} = 2G\left[e_{ij} + \frac{\nu}{1-2\nu}e_{kk}\delta_{ij} - \frac{(1+\nu)}{1-2\nu}\alpha(T-T_o)\delta_{ij}\right] \tag{4}$$

into equation (3), it is found that

$$\frac{dW}{dV} = \frac{1}{2E}\left[(1+\nu)\sigma_{ij}\sigma_{ij} - \nu\sigma_{kk}^2\right] \tag{5}$$

where ν is the Poisson's ratio and E the Young's modulus. Note that

the term involving $\Delta T = T-T_o$ does not appear when dW/dV is expressed in terms of the stress components. However, when σ_{ij} in equation (3) are eliminated by means of the strain-stress relation

$$e_{ij} = \frac{1+\nu}{E}\sigma_{ij} - \frac{\nu}{E}\sigma_{kk}\delta_{ij} + \alpha(T-T_o)\delta_{ij} \tag{6}$$

there results the expression:

$$\frac{dW}{dV} = G\left[e_{ij}e_{ij} + \frac{\nu}{1-2\nu}e_{kk}^2 - \frac{2(1+\nu)}{1-2\nu}\alpha(T-T_o)e_{kk}\right]$$

$$+ \frac{3G(1+\nu)}{1-2\nu}\alpha^2(T-T_o)^2 \tag{7}$$

Comparing equations (2) and (7), it is obvious that C_o is not zero and is equal to

$$C_o = \frac{3G(1+\nu)}{1-2\nu}\alpha^2(T-T_o)^2 \tag{8}$$

The omission of C_o can obviously lead to errors in predicting failure sites when using dW/dV as the failure criterion.

For nonlinear thermal elastic problems, equation (3) must be modified to take the form

$$\frac{dW}{dV} = \int_o^{\varepsilon_{ij}} \sigma_{ij}de_{ij} + f(\Delta T) \tag{9}$$

III. PREDICTION OF FRACTURE PATH

Sih and Kipp [3] have proposed that the initial notch and loading geometries (and material properties) may not only determine the failure load and initial fracture angle, but also the subsequent fracture path. They have shown that for a line crack in tension, the fracture path appears to follow a trajectory of points of relative minimum strain energy density. When local and global instability occur simultaneously, the energy state with reference to the initial configuration may determine the subsequent fracture path in some neighborhood. In such cases, crack growth occurs rapidly and the material has little time to follow the change in crack geometry for small time intervals. Hence, the prediction yields sufficiently accurate results for distances comparable to the half length of the crack or notch.

When the crack acquires a finite radius of curvature, the point of failure initiation is no longer obvious. The location on the blunted crack front or notch must be determined. To this end, the strain energy density in a surface layer energy has to be calculated [4]. Let the thickness of this layer be δ. The strain energy per unit surface layer area for plane strain can thus be written as

$$\gamma_e = \frac{1-\nu^2}{2E}\,\delta\sigma_t^2 \tag{10}$$

where σ_t is the local tangential stress. The quantity $2E\gamma_c/(1-\nu^2)$ can be regarded as a material parameter allowing failure loads to be cal-

culated. The location on the notch boundary at which failure occurs is assumed to coincide with the maximum value of γ_e or dW/dV. The surface thickness δ provides a means of considering surface inhomogeneities that are inherent in all materials. Inspection of equation (10) shows that γ_e does not observe the difference between regions of tensile and compressive tangential stress along the notch boundary. The sign of the tangential stress at the point of maximum strain energy density along the notch boundary may serve as a guide for determining the point of failure initiation. Positive tangential stress or tension may be assumed to coincide with the site of failure. Alternatively, experience tells us that fracture path tends to deviate in a direction normal to tension and to spread into the direction of compression. With this knowledge, the notch side at which failure initiates becomes obvious.

Once the point of failure initiation on the notch is known, the relative minima of the strain energy density or $(dW/dV)_{min}$ may be calculated for determining the fracture trajectories. To be more specific, a set of local polar coordinates (r,θ) is defined at the point of failure initiation as shown in Figure 1a. Hence, the values of dW/dV at all points near the notch front can be located. Figure 1b shows a typical set of constant dW/dV contours. A plot of dW/dV as a function of θ can thus be generated, Figure 1c. In general, there might be several $(dW/dV)_{min}$ values. The maximum relative minima, $(dW/dV)_{min}^{max}$, are selected as the locus of predicted fracture path.

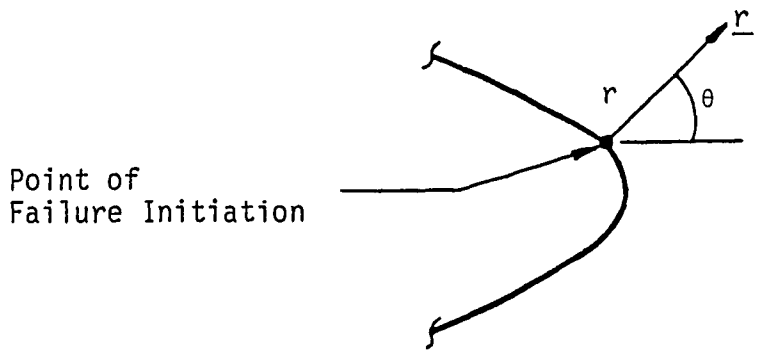

Figure 1(a) - Coordinate system originating at point of failure initiation [3]

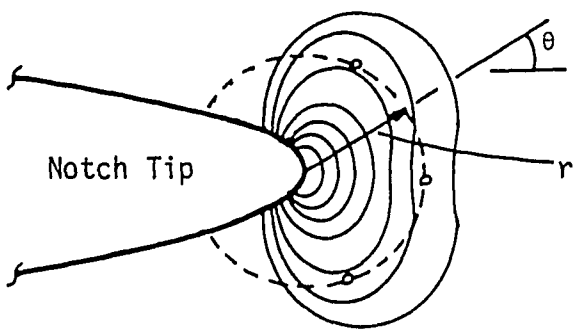

Figure 1(b) - Radius vector locus intersecting dW/dV contours [3]

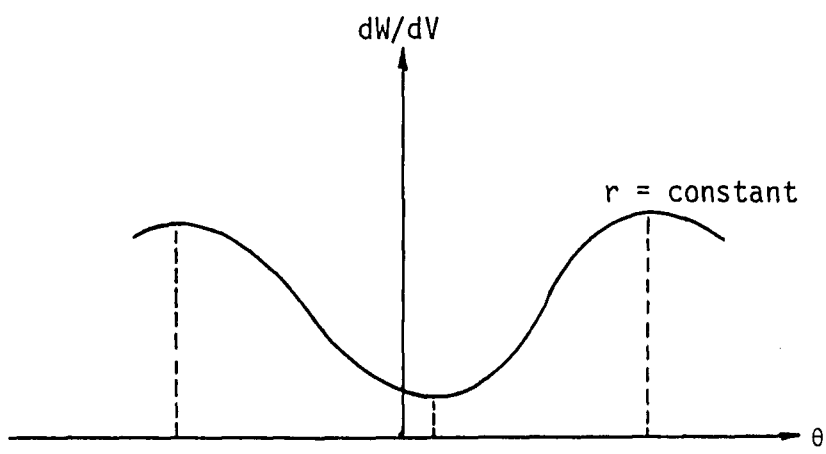

Figure 1(c) - Variation of dW/dV with polar angle θ
for constant magnitude radius vector [3]

IV. FINITE ELEMENT ANALYSIS

Finite element analysis is a method that spatially discretizes the mathematically assumed smooth continuum by a pre-conceived grid pattern. The grids may consist of a finite number of elements of different geometric shapes and sizes depending on the accuracies required in the various sub-regions. Such a discretization process invokes certain approximations on the solution of the differential equations that govern the behavior of the continuum in terms of stresses, displacements, temperatures, etc. The approximations depend on the size and distribution of the elements in relation to the rate at which load is being transmitted to the various sub-regions that may consist of different geometries and/or material properties. The procedure for pre-determining the degree of approximation, however, is not always clear.

Very briefly, the field variable at the nodal points of the elements is expressed in terms of the so-called "shape functions", say $N_i(x,y)$ in two dimensions. Then the field variable $a(x,y)$ can be expressed as

$$a(x,y) = \sum_{i=1}^{n} N_i(x,y)a_i(x,y) \tag{11}$$

where $a_i(x,y)$ are the nodal values of $a(x,y)$ and n is the number of nodes. To be considered in this work is the finite element formulation for steady state thermoelasticity. The governing equations can

be derived from the principle of Minimum Potential Energy [8] while the finite element formulations from the variational principles [9-11]. A system of linear algebraic equation of the form

$$\sum_{i=1}^{m} K_{ij} a_i = R_j \tag{12}$$

is obtained. In equation (12), a_i are the nodal values of the field variable, K_{ij} are the component of the global stiffness matrix, R_j is the global load vector and m is the total number of degrees of freedom of the system. This global system of equations is assembled from the finite element formulations for the individual elements.

The analysis consists of two parts: heat transfer and stress redistribution. The heat transfer portion is performed using a simple finite element code written by the author [12]. The finite element equations are derived from the variational principle following common procedures [11]. Linear shape functions are used with triangular elements. The system of equations is solved with a library subroutine [13] which uses a decomposition-substitution algorithm. The steady-state temperature distribution is input into a separate stress analysis program. Stress analysis is performed using a two-dimensional finite element computer program [14]. The APES (Axisymmetric/Planar Elastic Structures) program utilizes a 12 node isoparametric quadrilateral element having cubic shape functions. These elements assume a bicubic variation of the displacement field. A detailed explanation of the higher order isoparametric element can be found in Zienkiewicz

[9]. Numerical integration is performed using a 3x3 Gaussian quadrature. The APES program has a thermal stress analysis capability requiring the input of nodal temperatures. However, the version of APES used here calculates the out-of-plane stress σ_z incorrectly in the case of plane strain problems with thermal loading. The correct expression for σ_z is

$$\sigma_z = \nu(\sigma_x+\sigma_y) - E\alpha T \tag{13}$$

The program omits the term $E\alpha T$ which is only required in the case of plane strain [12].

The finite element equations are solved using the APES program. The nodal displacements and temperatures are input into a post-processing program. Strains, stresses and strain energy density are calculated at sampling point in the interior of the element and interpolated to other interior points or points on the element boundary. This results in improved accuracy and interelement continuity [9]. The sampling points used are the Gauss-Legendre quadrature points used in the numerical integrations. The interpolation functions used are the Legendre polynomials [15]. Thus, values of dW/dV can be determined for poing along the locus of a vector $\underline{r}$ of a given magnitude. Consequently, the $(dW/dV)_{min}$ paths can be determined from the numerical solution.

V. DISCUSSION OF RESULTS

A. UNIFORM HEAT FLOW PASSING A NARROW ELLIPTICAL NOTCH

In order to establish the validity of the finite element procedure, the problem of a narrow elliptical notch engulfed by an uniform heat flow is first solved numerically so that a comparison with the analytical solution of a line crack [2] can be made. The ratio of the semi-minor to semi-major axis of the ellipse is taken to be $b/a = 0.05$ and a condition of plane strain is assumed. Refer to Figures 2(a) and 2(b) for the geometric configurations and thermal boundary conditions of these two problems. Both the elliptical notch and crack are assumed to be insulated. The corresponding finite element grid patterns are given in Figures 3 and 4.

More specifically, temperature boundary conditions are specified at the edges $y = \pm L$:

$$(T(x,L) - T_0) = -T_1;\ (T(x,-L) - T_0) = T_1 \tag{14}$$

This results in a temperature distribution approximating that of uniform heat flow in regions far away from the crack and notch. This is shown in Figures 5(a) and 5(b). Note that the isotherms are more severely disturbed in the vicinity of the crack or notch. The temperature fields are symmetric with reference to both the x- and y-axis as defined in Figures 2(a) and 2(b). By means of equation (7), the strain energy density functions dW/dV are calculated for determining

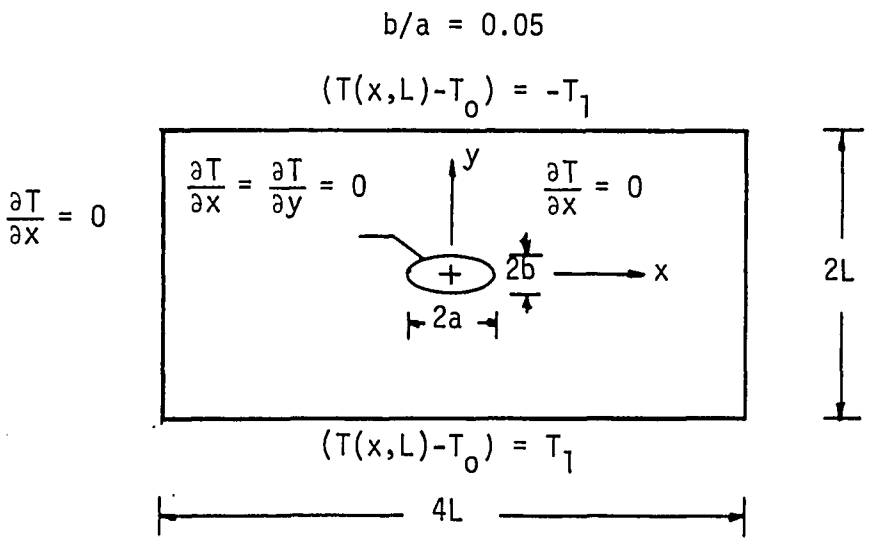

Figure 2(a) - Uniform heat flow past a narrow elliptical notch: geometry and boundary conditions

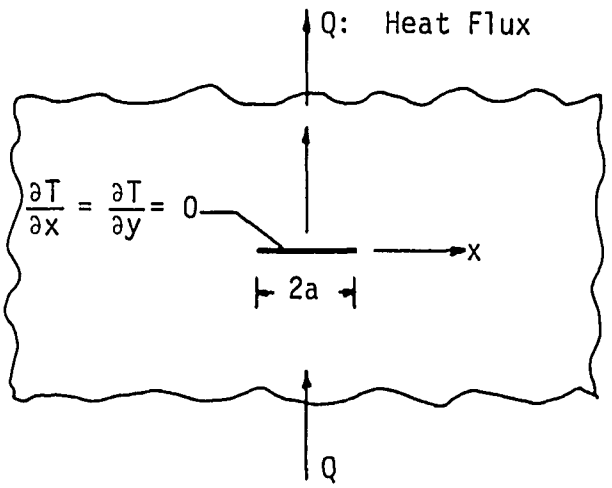

Figure 2(b) - Uniform heat past a line crack: geometry and boundary conditions

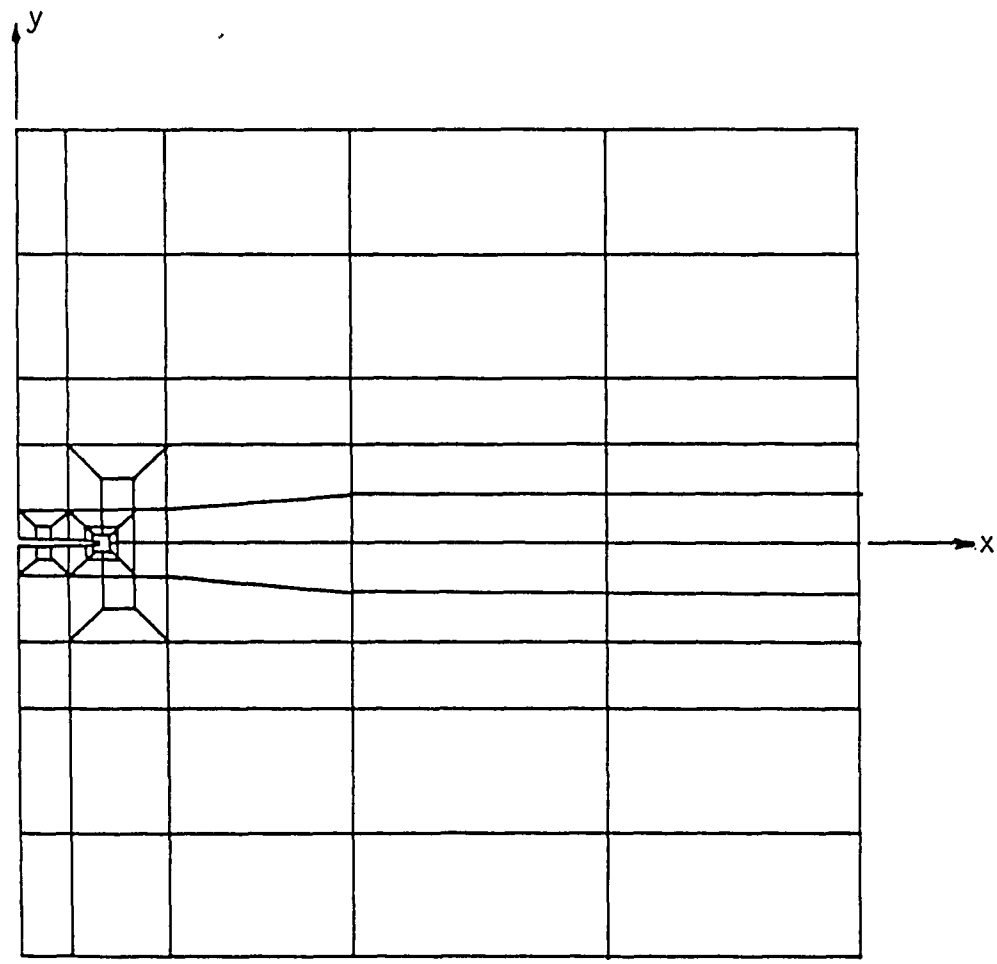

Figure 3 - Finite element grid for stress analysis of uniform heat flow past notch, 1/2 symmetry

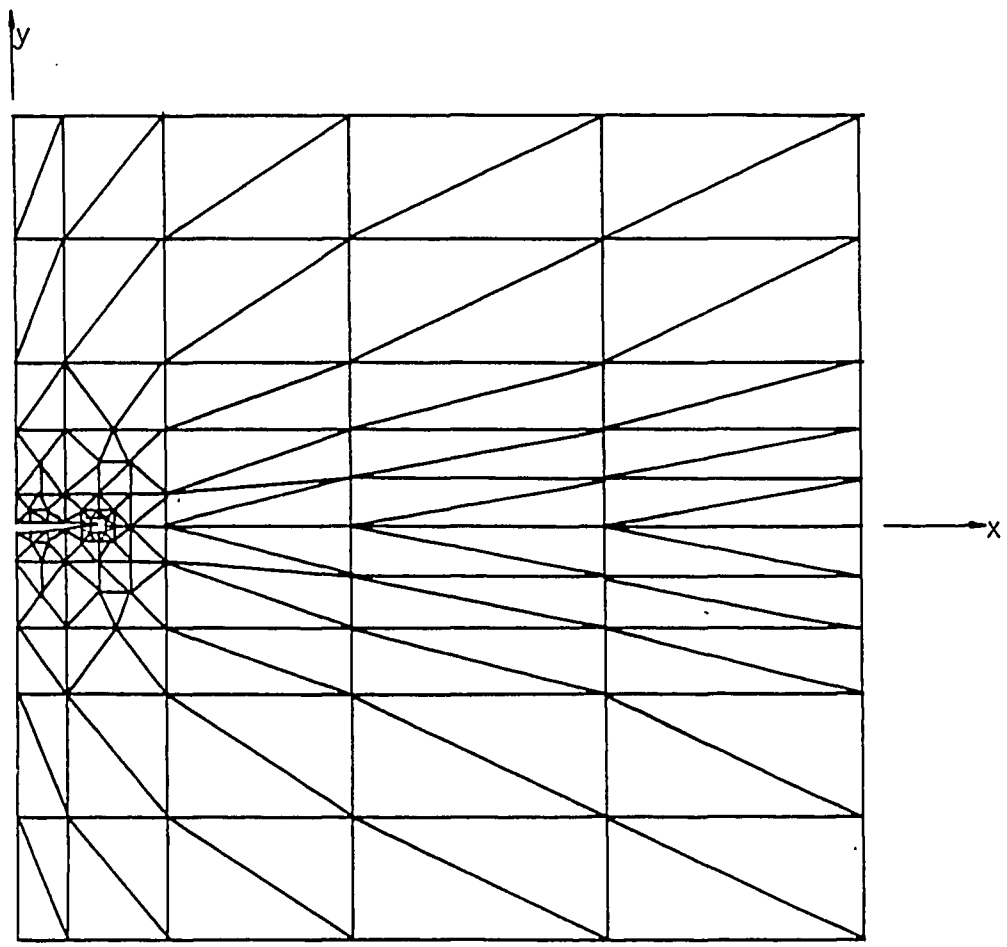

Figure 4 - Finite element grid for heat transfer analysis of uniform heat flow past notch, 1/2 symmetry

Temperature $(T-T_0)$

Contour Values

1 - -156.7°C

2 - -128.9°C

3 - -101.1°C

4 - - 73.3°C

5 - - 45.6°C

6 - - 17.8°C

7 - 10°C

8 - 37.8°C

9 - 65.5°C

10 - 93.3°C

11 - 121.1°C

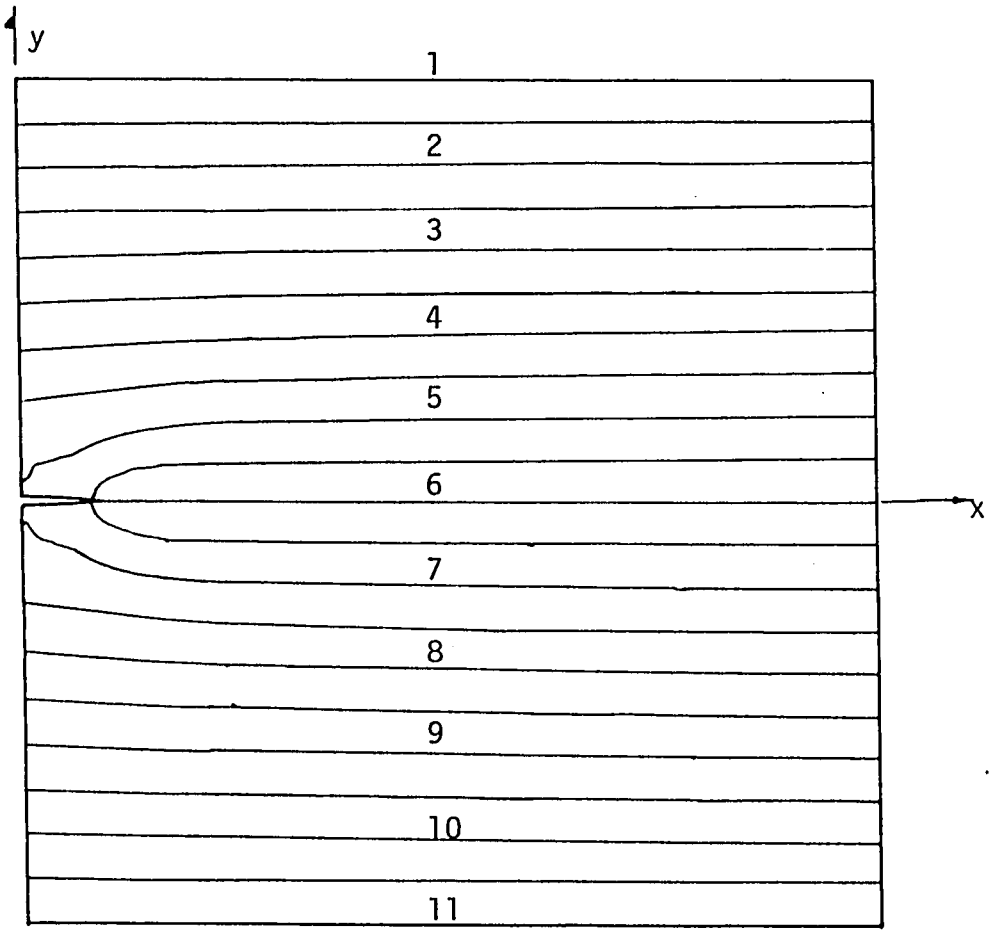

Figure 5(a) - Temperature distribution resulting from an uniform heat flow across a notch

Temperature ($T-T_o$)

Contour Values

1 - -121.1°C

2 - - 93.3°C

3 - - 65.5°C

4 - - 37.8°C

5 - - 10.0°C

6 - 0.0°C

7 - 10.0°C

8 - 37.8°C

9 - 65.5°C

10 - 93.3°C

11 - 121.1°C

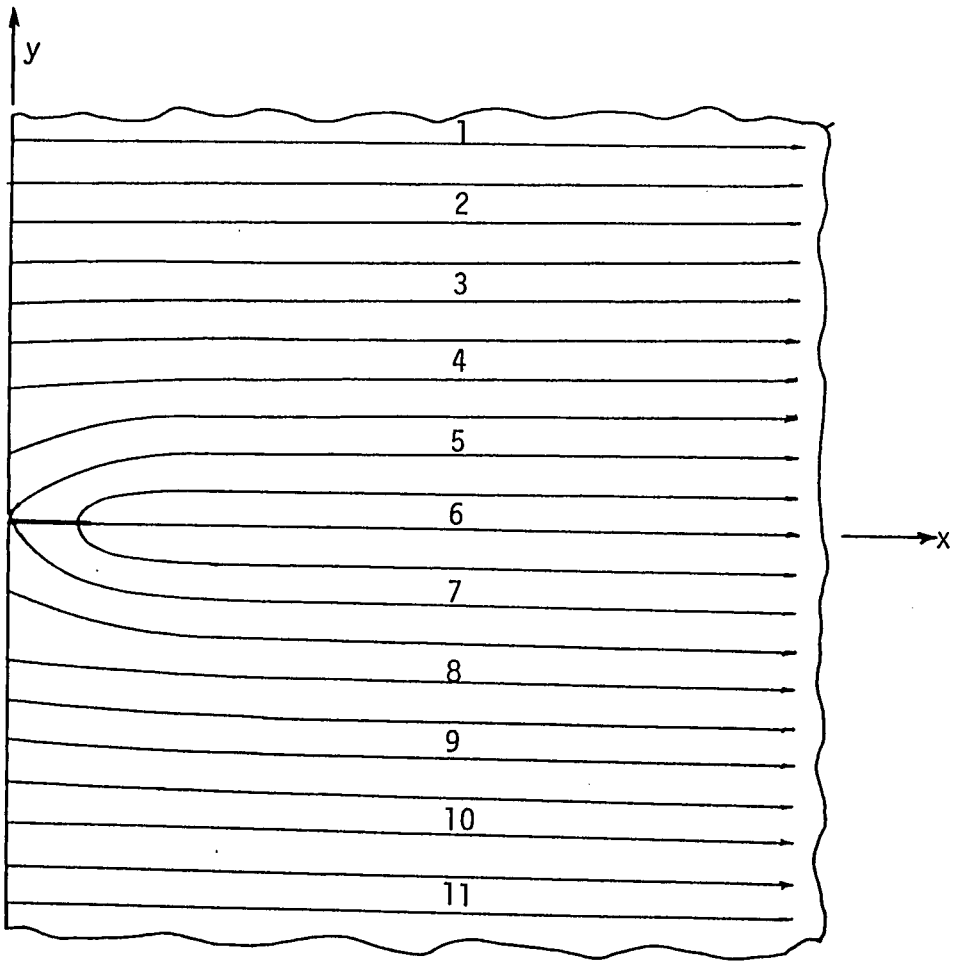

Figure 5(b) - Temperature distribution resulting from an uniform heat flow across a line crack [16]

their relative minima, i.e., values of (r,θ) corresponding to $(dW/dV)_{min}$ are obtained. The results are displayed in Figure 6(a) for the crack and Figure 6(b) for the notch. Two possible solutions of $(dW/dV)_{min}$ path prevails because dW/dV is a positive definite function that does not depend on the direction of heat flow. The choice of the correct path can be made on physical grounds that the material on the side with the lower temperature is in tension while compression is experienced by the material on the hotter side. Hence, the solid lines correspond to the correct crack trajectories. The dotted curves are also possible solutions when the direction of heat flow is reversed. Alternatively, it is also possible to determine the location of γ_e maximum in equation (10). In this case, point A in Figure 6(b) is thus selected to be the origin of failure and the upper path ($y>0$) is the probable fracture trajectory. Since the crack is the limiting case of the notch, the upper path is also selected for the case of a crack in Figure 6(a). The paths of $(dW/dV)_{min}$ for the crack and notch in Figures 6 are seen to be similar. Particular values of dW/dV along the paths can be found in Tables 1 and 2. The values of $(dW/dV)_{min}$ for the crack are higher because of the influence of the $1/\sqrt{r}$ singularity for the crack. The curvature of the fracture trajectory in Figure 6(a) is more pronounced than that in Figure 6(b). The close agreement between the analytical crack solution [2] and the numerical elliptical notch solution is encouraging. In the subsequent work, the procedure will be applied to other cases for which no analytical solution is available.

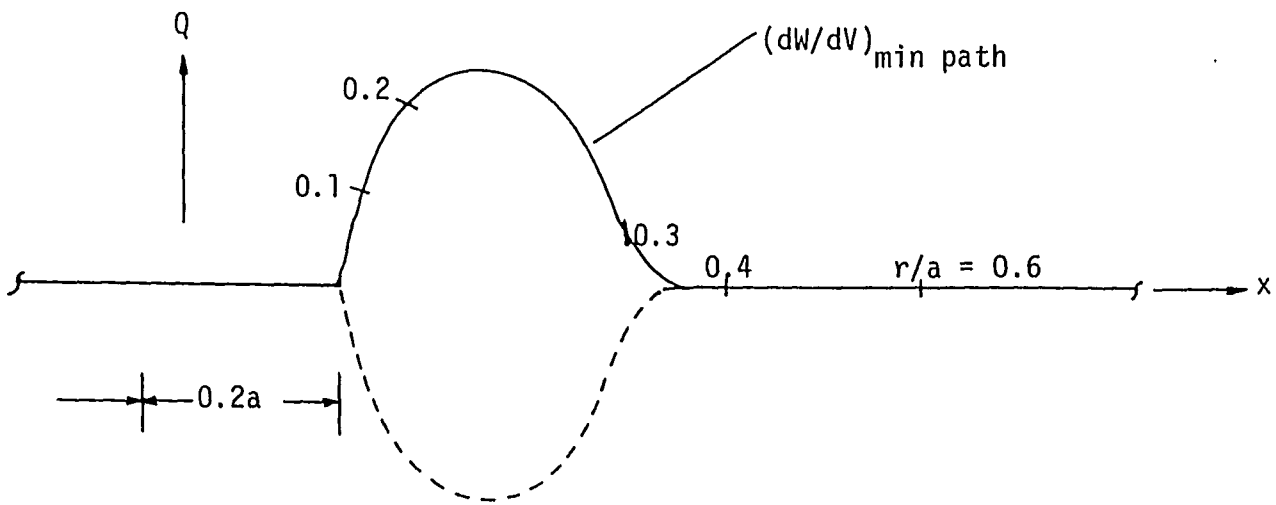

Figure 6(a) - Fracture trajectory emanating from a crack, b/a = 0.0 [2]

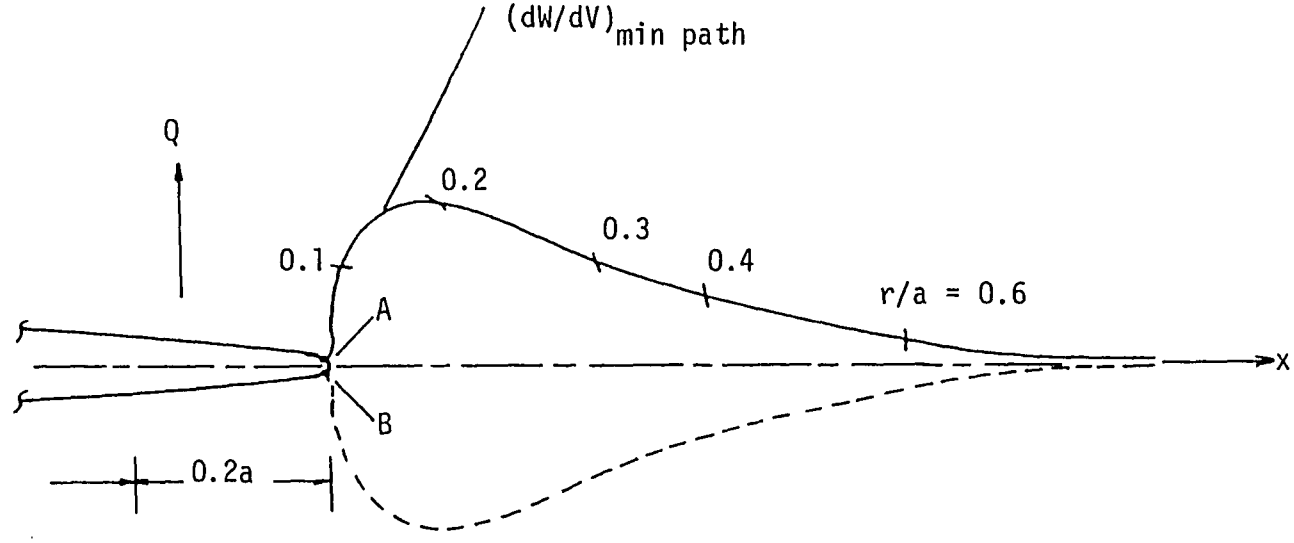

Figure 6(b) - Fracture trajectory emanating from a notch, b/a = 0.05

TABLE 1(a)

$\left(\frac{dW}{dV}\right)_{min}$ Values

Crack in Uniform Heat Flow, $C_o \neq 0$

r/a	θ	x/a	y/a	$\frac{1}{B}\left(\frac{dW}{dV}\right)^{max}_{min}$
0.01	-82	.0014	-.0099	18.8926
0.02	-82	.0028	-.0198	9.5015
0.03	-82	.0042	-.0297	6.3862
0.05	-82	.0070	-.0495	3.9220
0.07	-81	.0110	-.0691	2.8923
0.1	-80	.0174	-.0985	2.1553
0.2	-71	.0651	-.1891	1.4365
0.3	-35	.2457	-.1721	1.2371
0.4	0	.4000	0.0	.8982
0.8	0	.8000	0.0	.3849

$$B = \frac{1}{2} G[a\alpha Q_o]^2$$

TABLE 1(b)

$\left(\frac{dW}{dV}\right)_{min}$ Values

Crack in Uniform Heat Flow, $C_o=0$

r/a	θ	x/a	y/a	$\frac{1}{B}\left(\frac{dW}{dV}\right)^{max}_{min}$
0.01	278	.0014	-.0099	18.8701
0.02	278	.0028	-.0198	9.4562
0.03	278	.0042	-.0297	6.3178
0.05	278	.0070	-.0495	3.3806
0.07	278	.0097	-.0693	2.7295
0.1	278	.0139	-.0990	1.9209
0.2	278	.0278	-.1981	.9740
0.3	278	.0418	-.2971	.6546
0.4	278	.0557	-.3961	.4924
0.8	279	.1251	-.7902	.2383

$$B = \frac{1}{2} G[a\alpha Q_o]^2$$

TABLE 2(a)

$\left(\frac{dW}{dV}\right)_{min}$ Values

Check Problem, $C_o \neq 0$

r/a	θ	x/a	y/a	$\frac{1}{B}\left(\frac{dW}{dV}\right)^{max}_{min}$
Initiation Point		.998	.0032	12.9010
0.01	60	1.0029	.0119	2.6430
0.02	60	1.0077	.0207	1.8370
0.03	80	1.0032	.0323	1.2140
0.05	80	1.0067	.0524	.7712
0.07	80	1.0104	.0717	.5907
0.1	80	1.0153	.102	.4570
0.2	55	1.1127	.1673	.3121
0.3	20	1.280	.1064	.2442
0.4	10	1.392	.0745	.1776
0.8	0	1.8	0.0	.0572

$$B = \frac{1}{2} G\left[a\alpha \frac{T_1 - T_0}{L}\right]^2$$

TABLE 2(b)

$(\frac{dW}{dV})_{min}$ Values

Check Problem, $C_o=0$

r/a	θ	x/a	y/a	$\frac{1}{B}(\frac{dW}{dV})^{max}_{min}$
Initiation Point		.998	.0032	12.900
0.01	60	1.0029	.0119	2.6077
0.02	60	1.007	.0207	1.7844
0.03	80	.9957	.0332	1.1473
0.05	85	1.0020	.0530	.5480
0.07	90	.9980	.0732	.2774
0.1	90	.9980	.1030	- .0303
0.2	120	.8979	.1760	- .8069
0.3	140	.8469	.2640	-1.5210
0.4	155	.6359	.1721	-2.1901

$$B = \frac{1}{2} G[a\alpha \frac{T_1-T_0}{L}]^2$$

It is also of interest to note that a different failure path is predicted had C_o in equations (7) and (8) been neglected. Tables 1(b) and 2(b) give the values of $(dW/dV)_{min}$ for $C_o = 0$. Comparing with Table 1, the difference is significant.

B. EFFECT OF THERMAL AND MECHANICAL LOADING

The interaction of mechanical loading with thermal effects is investigated in this section. Figure 7 shows that, in addition to a temperature gradient in the positive y-direction, the cracked body is subjected to a tensile stress of magnitude σ. The elliptical notch is again assumed to be insulated. The finite element grid patterns are shown in Figures 8 and 9. Unlike the previous example where the temperatures at $y = \pm L$ are opposite in sign, symmetry in temperature no longer prevails for the present case of a general temperature gradient, Figure 10(a). Similarly, the resulting strain energy density distribution across the x-axis is also non-symmetric, Figure 10(b). Variations in the magnitude of mechanical loading relative to thermal effects will be studied in addition to changes in the b/a ratio. The influence of C_o in the calculation of dW/dV is also examined for all cases.

Let the ratio $\sigma/\alpha E\Delta T$ denote the proportion of mechanical to thermal load. Three $(dW/dV)_{min}$ constant lines are displayed in Figure 11 for b/a = 0.1 and $\sigma/\alpha E\Delta T$ = 0.00, 0.1026 and 0.3077. The predicted fracture path tends to shift toward the x-axis as the mechanical load is increased. This is to be expected since the fracture path is known

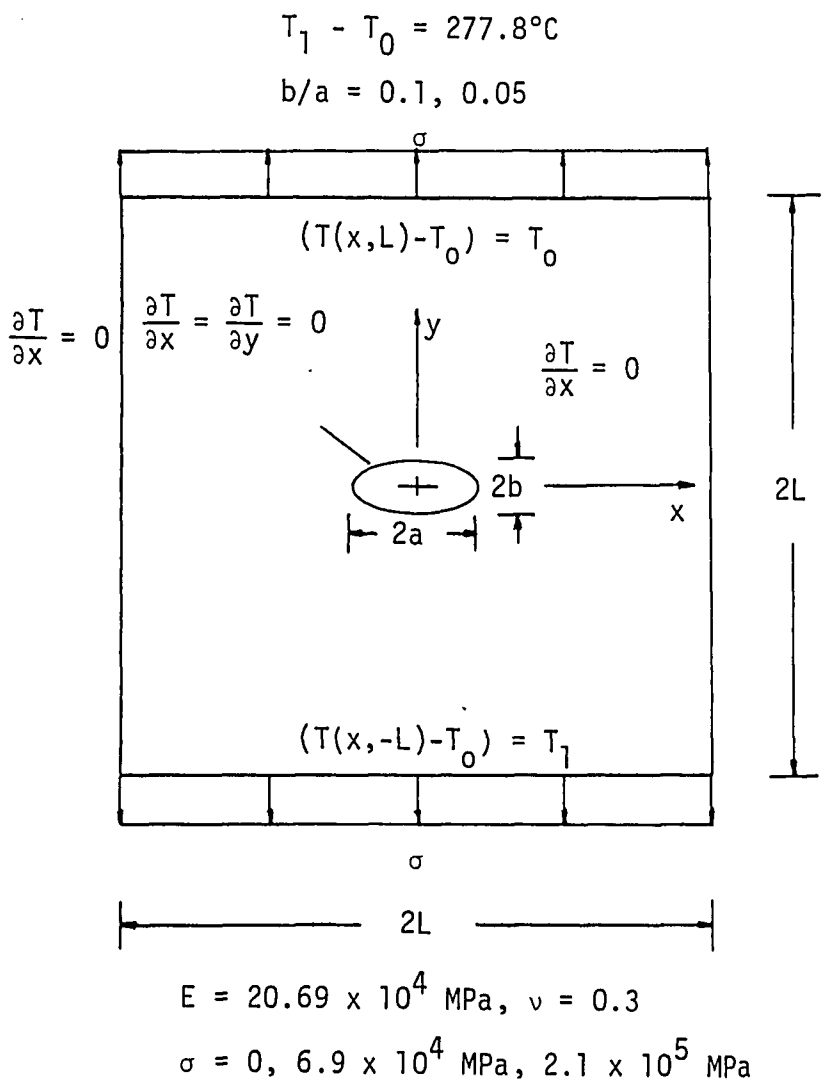

Figure 7 - Notch under combined mechanical and thermal loading: geometry and boundary conditions

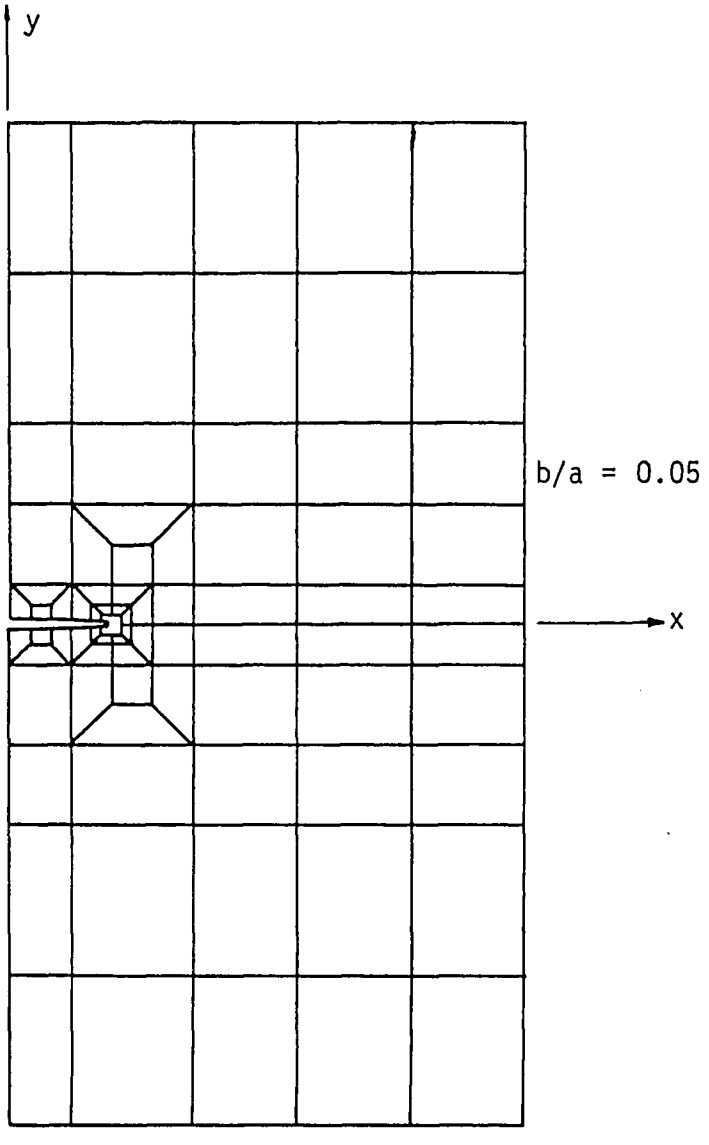

Figure 8(a) - Notch under combined mechanical and thermal loading: finite element grid for stress analysis, 1/2 symmetry

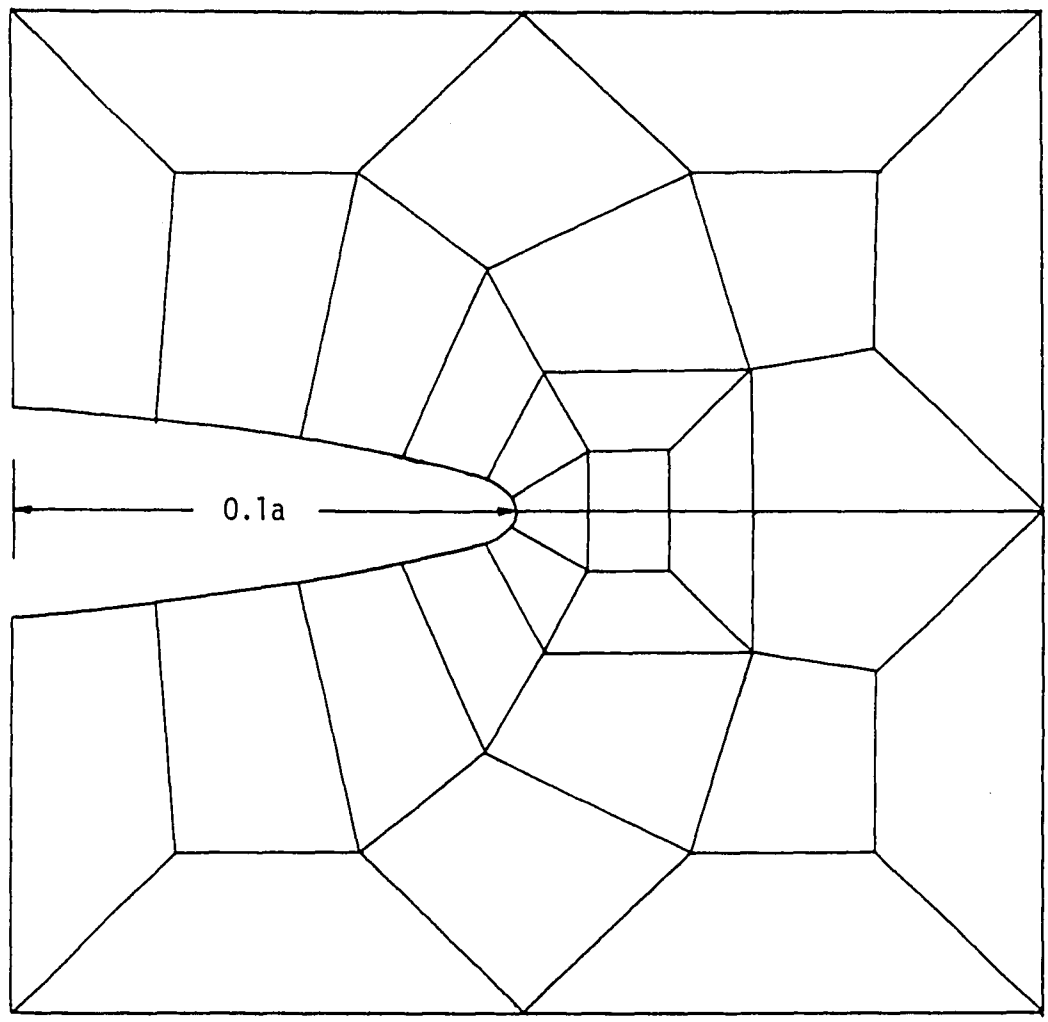

b/a = 0.05

Figure 8(b) - Close-up of notch tip finite element grid for stress analysis

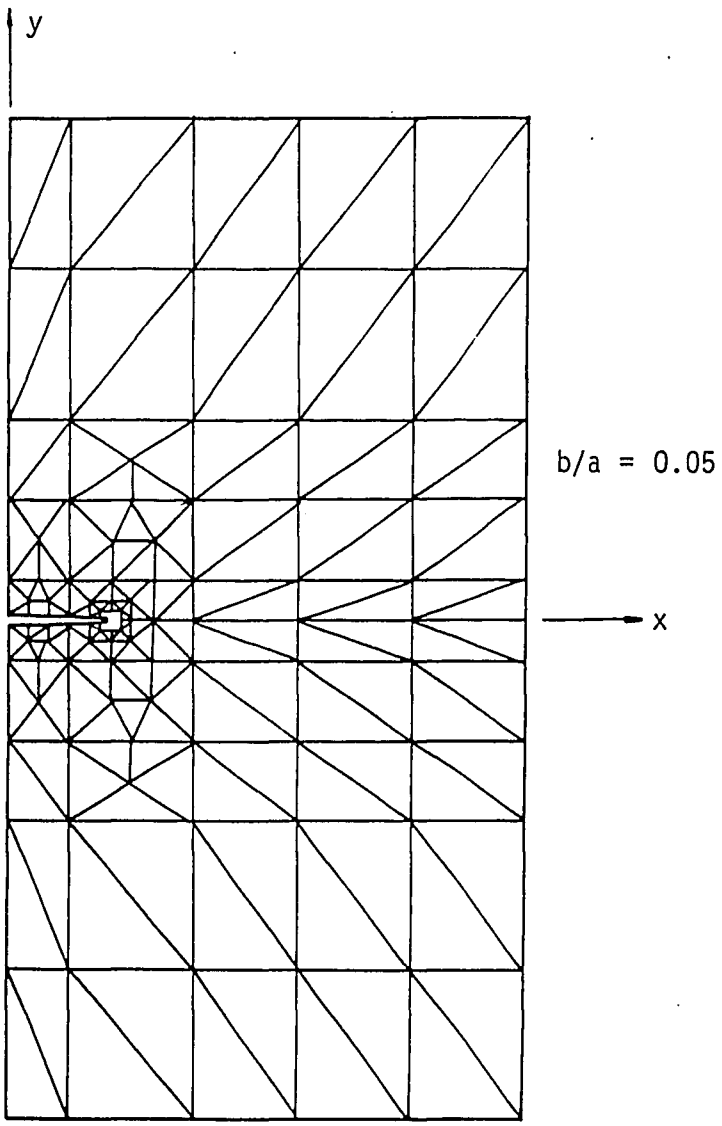

Figure 9(a) - Notch under combined mechanical and thermal loading: finite element grid for heat transfer analysis

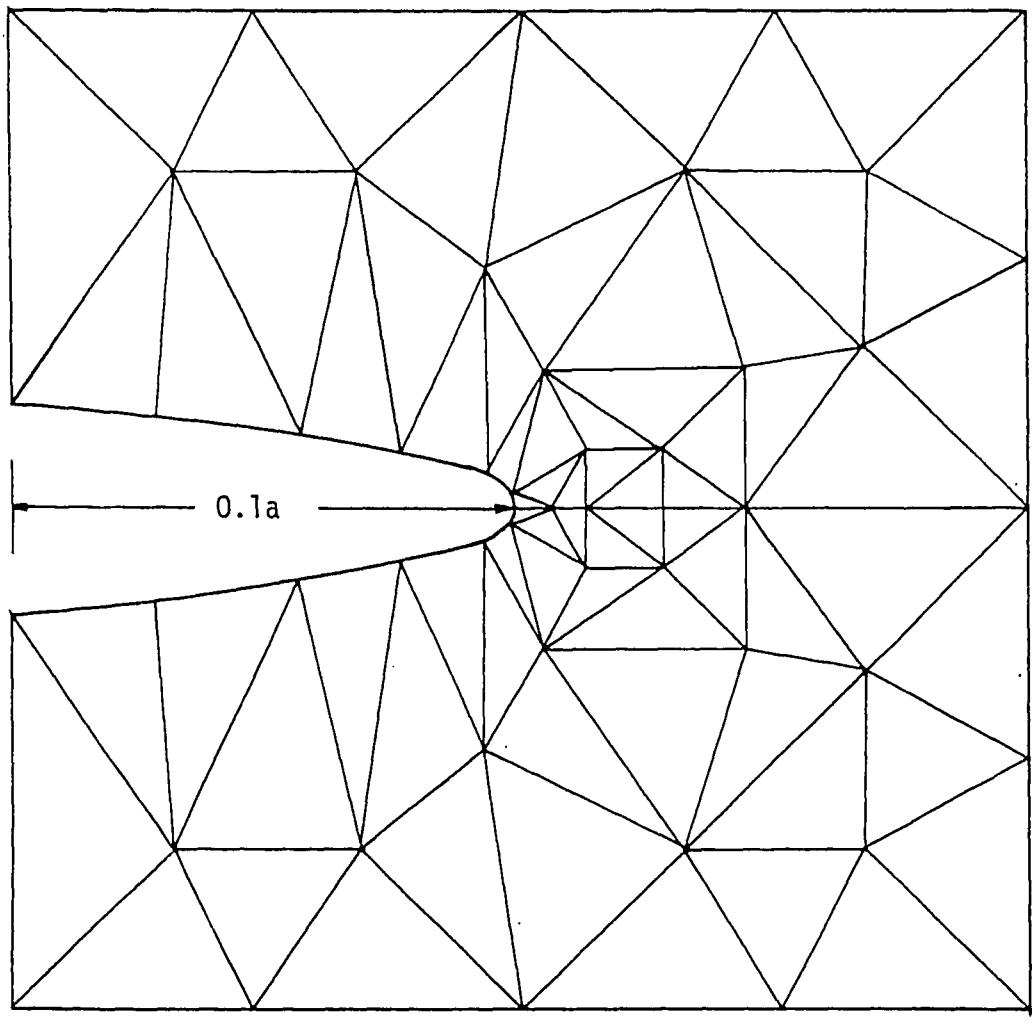

b/a = 0.05

Figure 9(b) - Close-up of notch tip finite element grid for heat transfer analysis

Temperature ($T-T_o$)

Contour Values

1 - -17.8°C

2 - 10.0°C

3 - 37.8°C

4 - 65.5°C

5 - 93.3°C

6 - 121.1°C

7 - 148.9°C

8 - 176.7°C

9 - 204.4°C

10 - 232.2°C

11 - 260.0°C

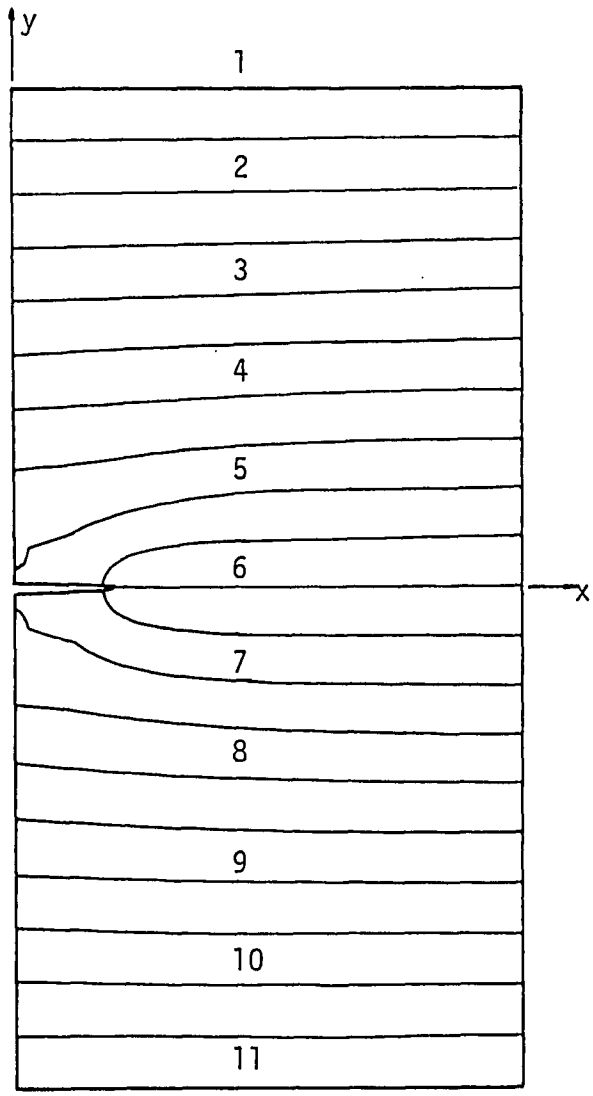

b/a = 0.05

Figure 10(a) - Temperature distribution resulting from a heat flow across an insulated notch: reference temperature on boundary

$\frac{1}{B}$ dW/dV

Contour Values

1 - 0.0

2 - 6.56

3 - 13.13

4 - 19.69

5 - 25.84

6 - 32.41

7 - 38.97

8 - 45.12

9 - 53.33

10 - 57.43

11 - 65.63

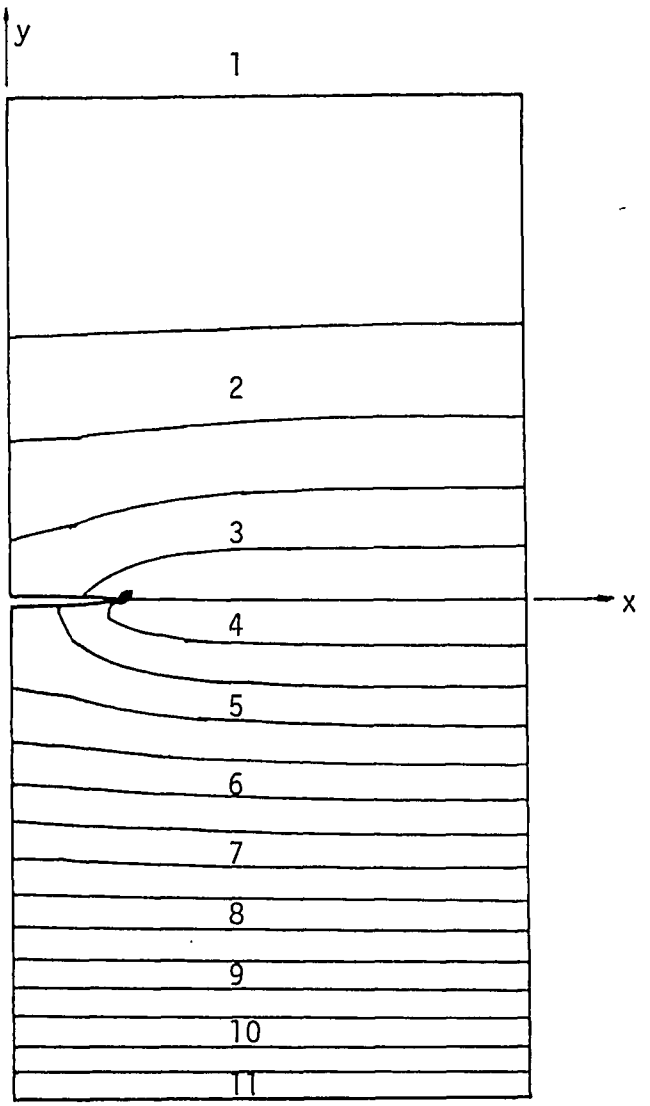

b/a = 0.05

Figure 10(b) - Strain energy density distribution resulting from temperature distribution in Figure 10(a), $\sigma/\alpha E\Delta T = 0$

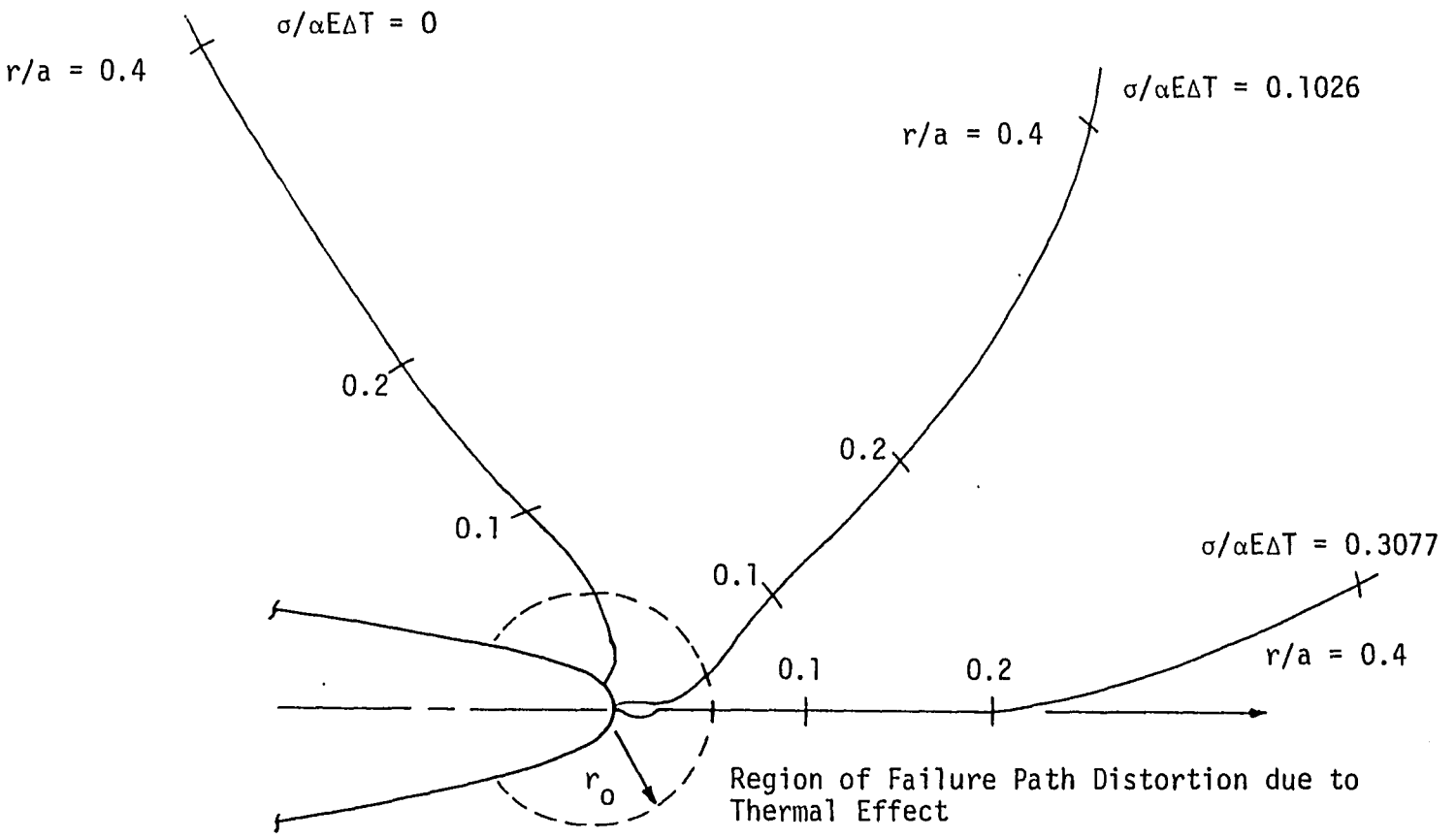

Figure 11 - Effect of the proportion of mechanical to thermal loading ($\sigma/\alpha E\Delta T$) on fracture trajectories, b/a = 0.1

by experience to coincide with the plane of symmetry for the mechanical load. Within a small region r_o, however, the failure path is seen to be highly distorted which indicates the localized effect of thermal loading. Figure 12 gives a plot of dW/dV/B against the distance r/a for different $\sigma/\alpha E\Delta T$ values. All the curves drop rapidly with distance near the notch tip. Here, the neglect of C_o yields to negative dW/dV which is obviously a violation of the law of thermodynamics. Refer to comparison of the values of $(dW/dV)_{min}$ in Tables 3 to 5 for $\sigma/\alpha E\Delta T$ = 0.0, 0.1026 and 0.3077, respectively.

Notch geometry is changed by varying the ratio of the minor axis of the notch to the major axis, b/a. An examination of the results in Tables 6 to 8 show that the primary effect of a change from b/a = 0.1 to b/a = 0.05 is to increase the intensity of the dW/dV field within a distance of r ≃ 0.02a from the origin of failure. This effect is stronger for the cases with higher applied tensile loads. The change in notch geometry from b/a = 0.1 to b/a = 0.05 also shifts the position of failure initiation toward the notch tip for the combinations of loading and geometry considered here.

C. INFLUENCE OF C_o ON FRACTURE PATH

As mentioned earlier, the term C_o in equation (7) can greatly influence the value and sign of dW/dV. This is seen in Figure 12 where dW/dV became negative when C_o was neglected, a result that is unacceptable in physics. This difference will be exhibited schematically in Figures 13 to 15 for three different ratios of $\sigma/\alpha E\Delta T$ with b/a = 0.1.

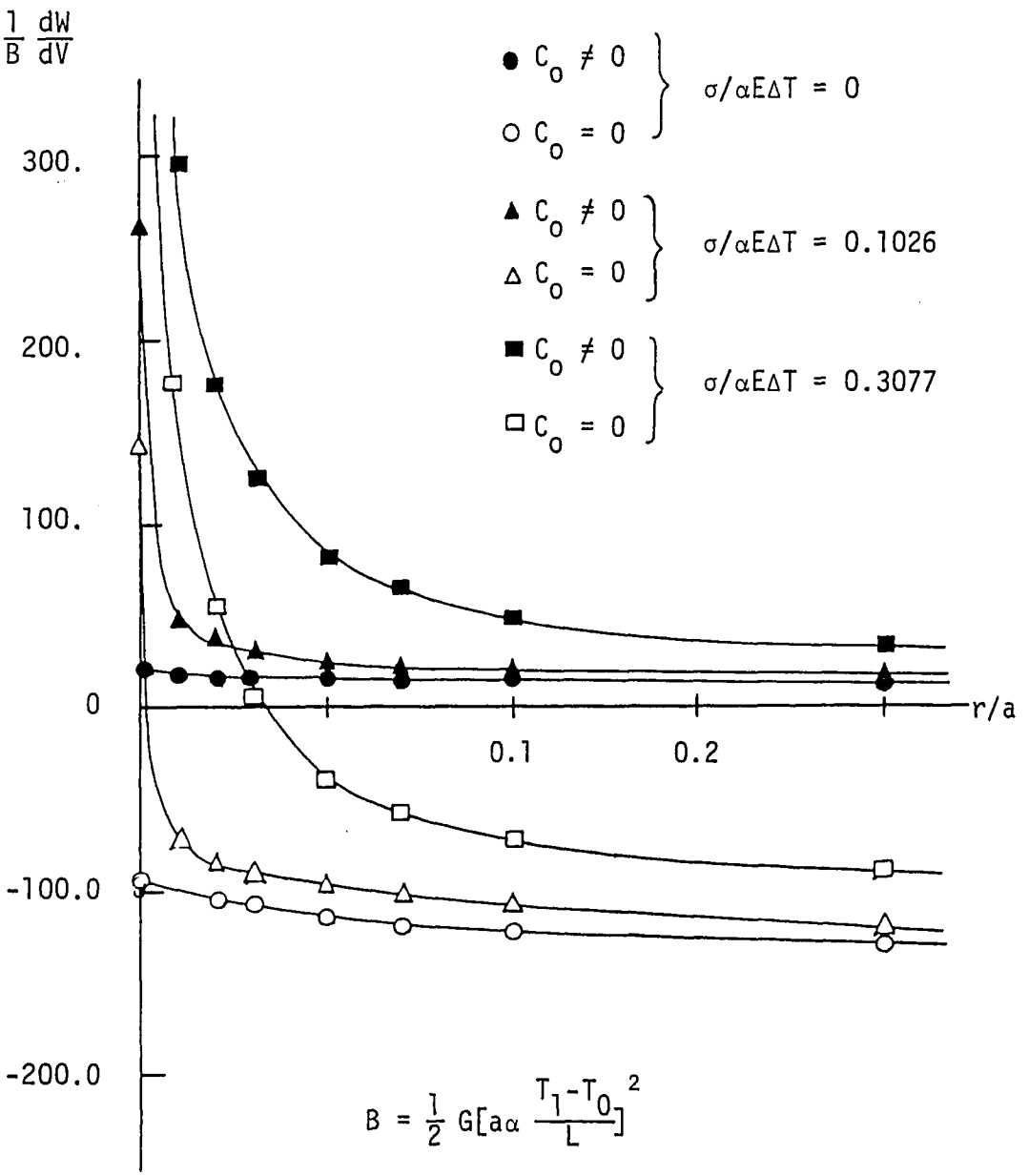

Figure 12 - Plot of $(dW/dV)_{min}/B$ versus r/a: effects of $\sigma/\alpha E\Delta T$ and C_o for b/a = 0.1

TABLE 3(a)

$\left(\frac{dW}{dV}\right)_{min}$ Values

Insulated Notch, b/a = 0.1, $\frac{\sigma}{E\alpha(T_1-T_0)}$ = 0.0, $C_0 \neq 0$

r/a	θ	x/a	y/a	$\frac{1}{B}\left(\frac{dW}{dV}\right)_{min}^{max}$
Initiation Point		.9926	.0122	21.9173
0.01	50	.9991	.02	17.2204
0.02	55	1.0041	.0286	16.5887
0.03	85	.9952	.0421	16.3672
0.05	90	.9925	.0622	15.3786
0.07	100	.9804	.0811	14.9110
0.1	110	.9580	.1062	14.3777
0.2	120	.8919	.1854	13.1963
0.4	120	.7910	.3583	11.7893

$$B = \frac{1}{2} G\left[a\alpha \frac{T_1-T_0}{L}\right]^2$$

TABLE 3(b)

$\left(\frac{dW}{dV}\right)_{min}$ Values

Insulated Notch, b/a = 0.1, $\frac{\sigma}{E\alpha(T_1-T_0)} = 0$, $C_o=0$

r/a	θ	x/a	y/a	$\frac{1}{B}\left(\frac{dW}{dV}\right)_{min}^{max}$
Initiation Point		.9926	.0122	- 94.1423
.01	- 50	.9990	.0045	-102.5515
.02	- 60	1.0024	-.0050	-104.3307
.03	- 75	1.0004	-.0168	-106.6535
.05	- 90	.9926	-.0378	-114.0372
.07	-100	.9804	-.0567	-118.9597
.1	-110	.9584	-.0818	-123.0618
.2	-130	.8640	-.1410	-129.6251
.4	-145	.6649	-.2172	-142.5466

$$B = \frac{1}{2} G\left[a\alpha \frac{T_1-T_0}{L}\right]^2$$

TABLE 4(a)

$\left(\frac{dW}{dV}\right)_{min}$ Values

Insulated Elliptical Notch, b/a = 0.1, $\frac{\sigma}{E\alpha(T_1-T_0)}$ = .1026, $C_0 \neq 0$

r/a	θ	x/a	y/a	$\frac{1}{B}\left(\frac{dW}{dV}\right)^{max}_{min}$
Initiation Point		.9999	.0014	261.5063
0.01	25	1.0092	.0056	47.5839
0.02	5	1.02	.0030	36.1063
0.03	20	1.028	.0115	29.0426
0.05	20	1.0469	.0189	23.7755
0.07	30	1.0605	.0363	21.2610
0.1	40	1.0767	.0656	19.6509
0.2	40	1.1542	.1285	17.1835
0.4	50	1.257	.3079	14.9725

$$B = \frac{1}{2} G\left[a\alpha \frac{T_1-T_0}{L}\right]^2$$

TABLE 4(b)

$\left(\frac{dW}{dV}\right)_{min}$ Values

Insulated Notch, b/a = 0.1, $\frac{\sigma}{E\,(T_1-T_0)}$ = .1026, C_o=0

r/a	θ	x/a	y/a	$\frac{1}{B}\left(\frac{dW}{dV}\right)_{min}^{max}$
Initiation Point		.9999	.0014	140.2904
0.01	25	1.0092	.0056	- 72.6885
0.02	0	1.02	.0015	- 85.2408
0.03	0	1.03	.0015	- 91.5990
.05	- 20	1.0472	-.0159	- 97.3008
.07	- 25	1.0635	-.0284	-101.1978
.1	- 45	1.0706	-.0693	-106.4484
.2	- 85	1.0173	-.1978	-120.6005
.4	-115	.8309	-.3611	-138.6496

$$B = \frac{1}{2} G\left[a\alpha \frac{T_1-T_0}{L}\right]^2$$

TABLE 5(a)

$\left(\frac{dW}{dV}\right)_{min}$ Values

Insulated Notch, b/a = 0.1, $\frac{\sigma}{E\alpha(T_1-T_0)}$ = .3077, $C_0 \neq 0$

r/a	θ	x/a	y/a	$\frac{1}{B}\left(\frac{dW}{dV}\right)^{max}_{min}$
Initiation Point		1.0	0.0	2158.0934
0.01	-20	1.0095	- .0034	296.4969
0.02	0	1.02	0.0	175.3220
0.03	0	1.03	0.0	126.6716
0.05	0	1.05	0.0	81.3438
0.07	0	1.07	0.0	64.0742
0.1	0	1.1	0.0	47.9121
0.2	0	1.2	0.0	33.1446
0.4	10	1.3917	.0653	26.6880

$$B = \frac{1}{2} G\left[a\alpha \left(\frac{T_1-T_0}{L}\right)\right]^2$$

TABLE 5(b)

$\left(\frac{dW}{dV}\right)_{min}$ Values

Insulated Notch, b/a = 0.1, $\frac{\sigma}{E\alpha(T_1-T_0)}$ = .3077, C_o=0

r/a	θ	x/a	y/a	$\frac{1}{B}\left(\frac{dW}{dV}\right)^{max}_{min}$
Initiation Point		1.0	0.0	2036.2622
0.01	-20	1.0095	- .0034	173.6402
0.02	0	1.02	0.0	53.4909
0.03	0	1.03	0.0	4.8076
0.05	0	1.05	0.0	- 40.5160
0.07	0	1.07	0.0	- 57.7980
0.1	0	1.1	0.0	- 73.9601
0.2	0	1.2	0.0	- 88.7275
0.4	-30	1.3464	- .200	- 103.5770

$$B = \frac{1}{2} G\left[a\alpha \frac{T_1-T_0}{L}\right]^2$$

TABLE 6(a)

$\left(\frac{dW}{dV}\right)_{min}$ Values

Insulated Notch, b/a = 0.05, $\frac{\sigma}{E\alpha(T_1-T_0)} = 0$, $C_o \neq 0$

r/a	θ	x/a	y/a	$\frac{1}{B}\left(\frac{dW}{dV}\right)^{max}_{min}$
Initiation Point		.998	.0032	29.1164
0.01	60	1.0029	.0119	18.4018
0.02	65	1.0065	.0213	17.4338
0.03	80	1.00295	.0328	16.4575
0.05	90	.9982	.0532	15.5796
0.07	100	.9859	.0722	15.1079
0.1	110	.9638	.0973	14.5418
0.2	120	.8979	.1750	13.3645
0.4	120	.7980	.3496	12.1421

$$B = \frac{1}{2} G\left[a\alpha \frac{T_1-T_o}{L}\right]^2$$

TABLE 6(b)

$\left(\frac{dW}{dV}\right)_{min}$ Values

Insulated Notch, b/a = 0.05, $\frac{\sigma}{E\alpha(T_1-T_0)} = 0$, $C_o=0$

r/a	θ	x/a	y/a	$\frac{1}{B}\left(\frac{dW}{dV}\right)_{min}^{max}$
Initiation Point		.998	.0032	- 89.96
.01	40	1.0057	.0097	- 99.68
.02	- 20	1.0168	-.0036	-101.98
.03	- 55	1.0152	-.0214	-107.88
.05	- 80	1.0067	-.0460	-112.81
.07	- 95	.9919	-.0665	-116.50
.1	-110	.9638	-.0908	-118.96
.2	-125	.8833	-.1606	-128.80
.4	-140	.6916	-.2539	-139.88

$$B = \frac{1}{2} G\left[a\alpha \frac{T_1-T_0}{L}\right]^2$$

TABLE 7(a)

$\left(\frac{dW}{dV}\right)_{min}$ Values

Insulated Notch, b/a = 0.05, $\frac{\sigma}{E\alpha(T_1-T_0)}$ = .1026, $C_o \neq 0$

r/a	θ	x/a	y/a	$\frac{1}{B}\left(\frac{dW}{dV}\right)_{min}^{max}$
Initiation Point		1.0000	.0002	464.2547
0.01	30	1.0086	.0049	30.2404*
0.02	15	1.0193	.0053	36.3155
0.03	20	1.0284	.0103	28.2755
0.05	25	1.0453	.0211	23.4884
0.07	30	1.0606	.0355	21.0231
0.1	40	1.0766	.0643	19.5463
0.2	40	1.1542	.1285	17.1712
0.4	55	1.2294	.3279	14.9725

$$B = \frac{1}{2} G\left[a\alpha \frac{T_1-T_0}{L}\right]^2$$

*This value is obviously non-physical and seems to be a numerical abbreviation; it is included as part of the consistent application of the theory in Section II.

TABLE 7(b)

$\left(\frac{dW}{dV}\right)_{min}$ Values

Insulated Notch, b/a = .05, $\frac{\sigma}{E\alpha(T_1-T_0)}$ = .1026, C_0=0

r/a	θ	x/a	y/a	$\frac{1}{B}\left(\frac{dW}{dV}\right)^{max}_{min}$
Initiation Point		1.0000	.0002	342.5219
.01	30	1.0086	.0049	- 90.1633*
.02	0	1.0200	0.0	- 84.8716
.03	10	1.0297	.0054	- 91.7220
.05	0	1.0499	0.0	- 97.0137
.07	- 20	1.0657	- .0237	-100.9107
.1	- 35	1.0818	- .0572	-104.3974
.2	- 75	1.0517	- .1930	-119.3699
.4	-105	0.8964	- .3862	-136.5986

$$B = \frac{1}{2} G\left[a\alpha \frac{T_1-T_0}{L}\right]^2$$

*This value is obviously non-physical and seems to be a numerical abbreviation; it is included as part of the consistent application of the theory in Section II.

TABLE 8(a)

$\left(\frac{dW}{dV}\right)_{min}$ Values

Insulated Notch, b/a = 0.05, $\frac{\sigma}{E\alpha(T_1-T_0)}$ = .3077, $C_o \neq 0$

r/a	θ	x/a	y/a	$\frac{1}{B}\left(\frac{dW}{dV}\right)^{max}_{min}$
Initiation Point		1.0		3819.0171
.01	-25	1.0089	- .0041	241.0789
.02	-40	1.0152	- .0127	214.3326
.03	-30	1.0259	- .0150	153.7042
.05	0	1.0500	0.0	78.8416
.07	10	1.0689	.0126	60.6695
.1	0	1.1	0.0	46.9276
.2	0	1.2	0.0	32.7180
.4	5	1.3990	.0349	26.7044

$$B = \frac{1}{2} G\left[a\alpha \frac{T_1-T_0}{L}\right]^2$$

TABLE 8(b)

$\left(\frac{dW}{dV}\right)_{min}$ Values

Notch Insulated, b/a = 0.05, $\frac{\sigma}{E\alpha(T_1-T_0)}$ = .3077, C_o=0

r/a	θ	x/a	y/a	$\frac{1}{B}\left(\frac{dW}{dV}\right)^{max}_{min}$
Initiation Point		1.0	0.0	3697.1860
.01	-25	1.0089	- .0041	117.9752
.02	-40	1.0152	- .0127	89.4249
.03	-30	1.0259	- .0150	28.8744
.05	0	1.05	0.0	- 43.0306
.07	0	1.07	0.0	- 59.9311
.1	0	1.1	0.0	- 74.9036
.2	0	1.2	0.0	- 89.1377
.4	-25	1.3625	- .1690	- 101.3209

$$B = \frac{1}{2} G\left[a\alpha \frac{T_1-T_0}{L}\right]^2$$

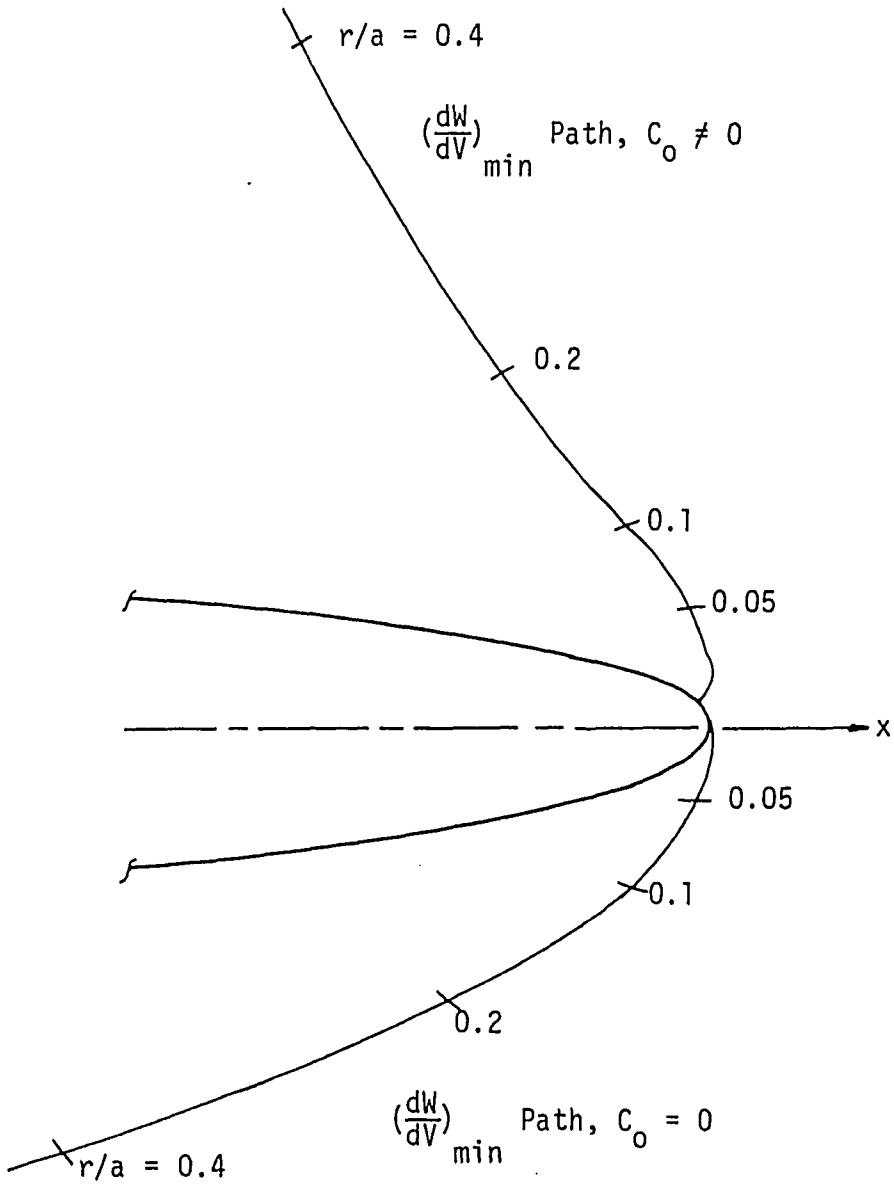

Figure 13 - Fracture trajectories for $C_o \neq 0$, $C_o = 0$, $\sigma/\alpha E\Delta T = 0$, $b/a = 0.1$

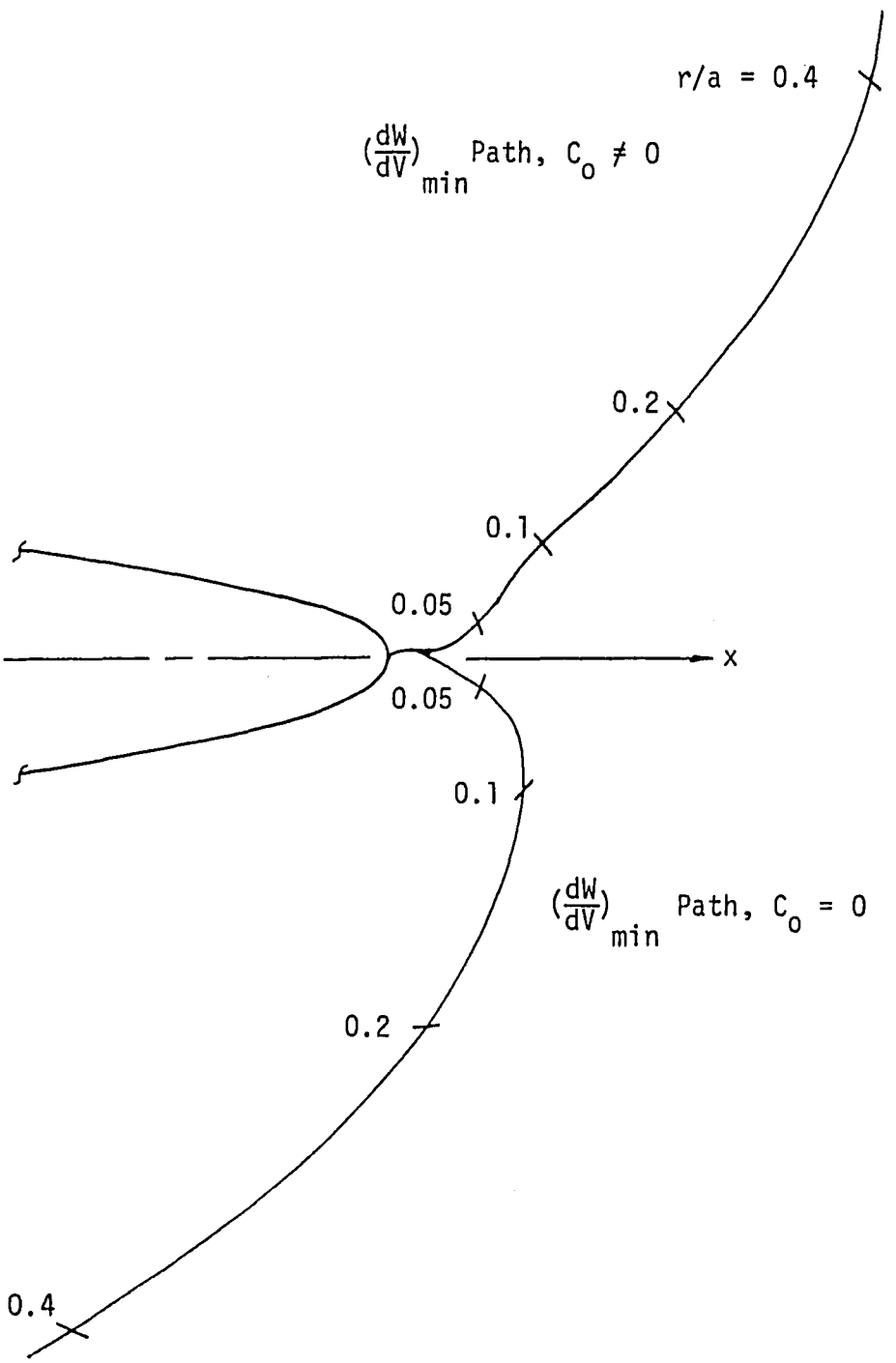

Figure 14 - Fracture trajectories for $C_o \neq 0$, $C_o = 0$, $\sigma/\alpha E\Delta T = 0.1026$, $b/a = 0.1$

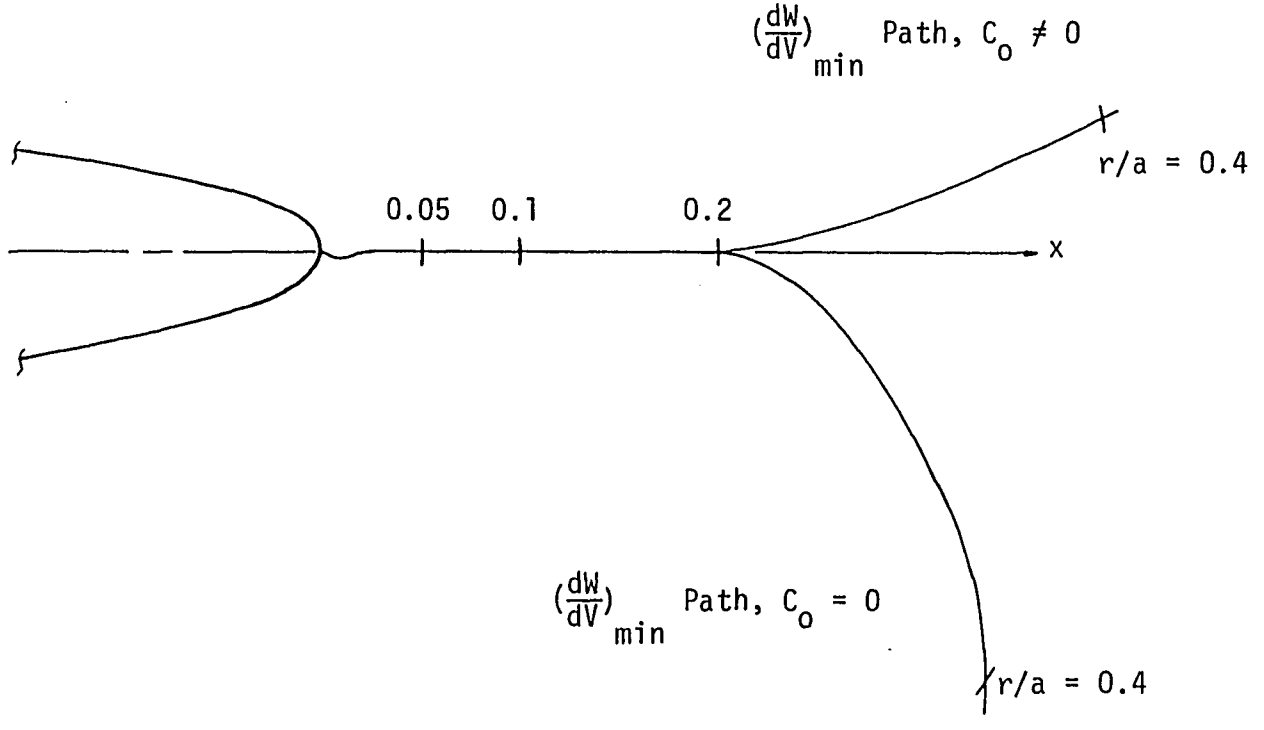

Figure 15 - Fracture trajectories for $C_o \neq 0$, $C_o = 0$, $\sigma/\alpha E\Delta T = 0.3077$, $b/a = 0.1$

In the absence of mechanical loading $\sigma/\alpha E\Delta T = 0$, Figure 13 shows that the predicted paths for $C_o \neq 0$ and $C_o = 0$ are in opposite direction. When mechanical load is applied with $\sigma/\alpha E\Delta T = 0.1026$, the initial portion of the crack trajectories for $C_o \neq 0$ and $C_o = 0$ are in close agreement while the derivations became significant at distances away from the notch. This is clearly shown in Figure 14. Further increase in the magnitude of mechanical loading, i.e., with $\sigma/\alpha E\Delta T = 0.3077$, the region within which the two curves for $C_o \neq 0$ and $C_o = 0$ coincide increase accordingly, Figure 15.

An example problem with a symmetric temperature distribution is also considered. Constant temperature boundary conditions are applied to both the outer boundary and the notch surface, Figure 16(a). This example could be used to model the physical problem of a leak of hot gas through a pressurized vessel whose radius of curvature is large in comparison with the notch length 2a, and when the temperature variation in the thickness direction is negligibly small. A tensile load is applied at the boundaries with $\sigma/\alpha E\Delta T = .5128$. Even though the predicted failure paths for $C_o \neq 0$ and $C_o = 0$ coincided in Figure 16 (b), the $(dW/dV)_{min}$ solution corresponding to $C_o = 0$ is unacceptable on physical grounds because the $(dW/dV)_{min}$ values are negative. Refer to the data in Tables 9(a) and 9(b).

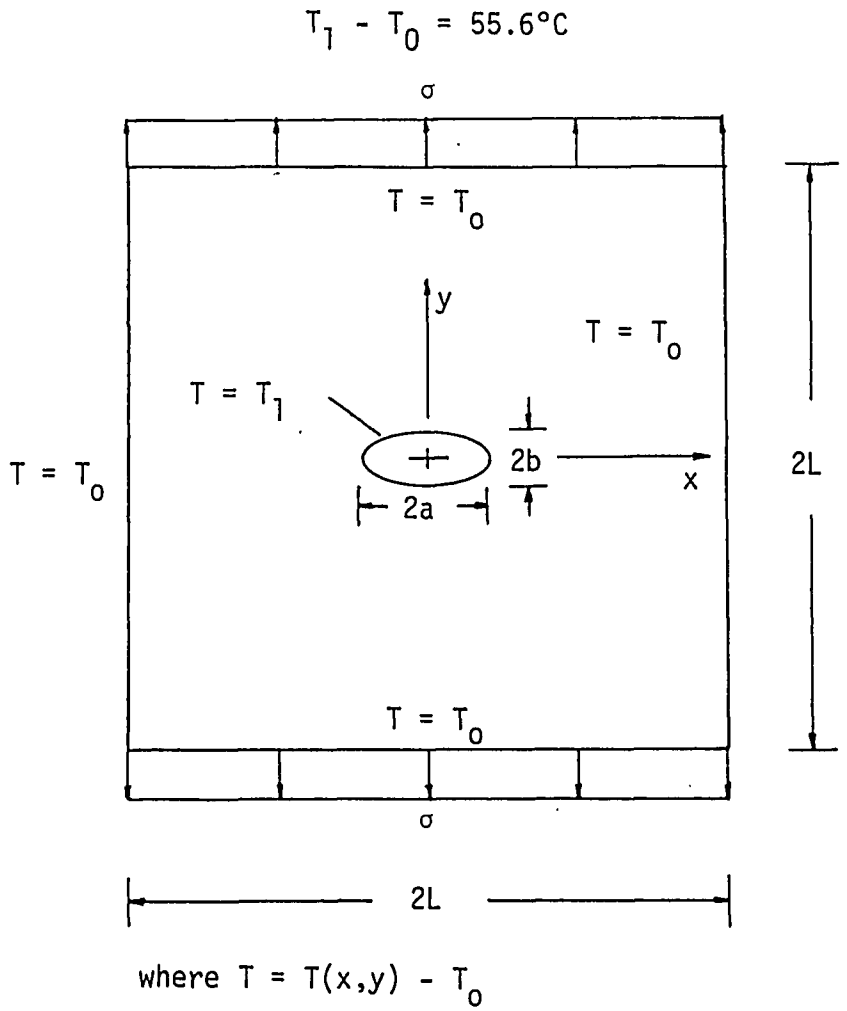

Figure 16(a) - "Leak problem": geometry and boundary conditions

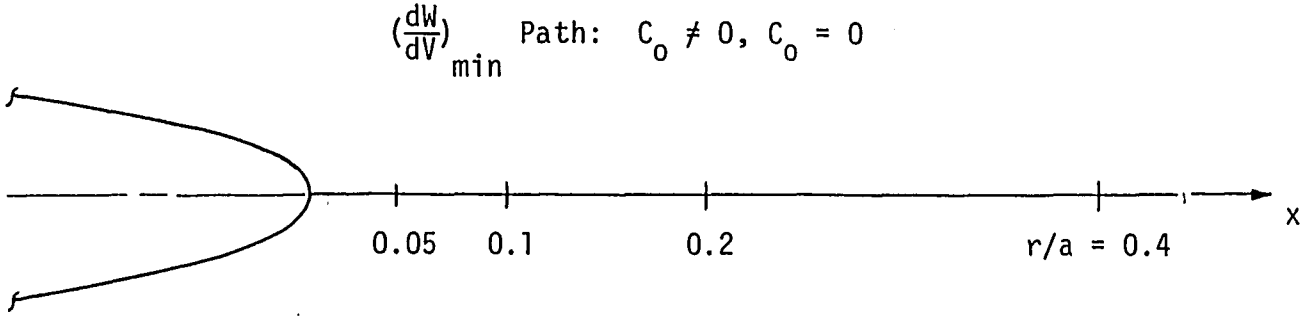

Figure 16(b) - Fracture trajectories for "leak problem",
$\sigma/\alpha E\Delta T = 0.5128$, $b/a = 0.05$

TABLE 9(a)

$\left(\frac{dW}{dV}\right)_{min}$ Values

"Leak Problem", b/a = 0.05, $\frac{\sigma}{E\alpha(T_1-T_0)}$ = .5128, $C_o \neq 0$

r/a	θ	x/a	y/a	$\frac{1}{B}\left(\frac{dW}{dV}\right)_{min}^{max}$
Initiation Point		1.0	0.0	505.6
0.01	0	1.01	0.0	76.88
0.02	0	1.02	0.0	73.29
0.03	0	1.03	0.0	72.22
0.05	0	1.05	0.0	69.11
0.07	0	1.07	0.0	67.24
0.1	0	1.1	0.0	65.20
0.2	0	1.2	0.0	59.61
0.4	0	1.4	0.0	52.83

$$B = \frac{1}{2} G\left[a\alpha \frac{T_1-T_0}{L}\right]^2$$

TABLE 9(b)

$\left(\frac{dW}{dV}\right)_{min}$ Values

"Leak Problem", b/a = 0.05, $\frac{\sigma}{E\alpha(T_1-T_0)}$ = .5128, C_o=0

r/a	θ	x/a	y/a	$\frac{1}{B}\left(\frac{dW}{dV}\right)^{max}_{min}$
Initiation Point		1.0	0.0	18.09
0.01	0	1.01	0.0	-376.87
0.02	0	1.02	0.0	-358.15
0.03	0	1.03	0.0	-339.79
0.05	0	1.05	0.0	-313.85
0.07	0	1.07	0.0	-292.31
0.1	0	1.1	0.0	-272.00
0.2	0	1.2	0.0	-220.62
0.4	0	1.4	0.0	-155.18

$$B = \frac{1}{2}\left[a\alpha\,\frac{T_1-T_0}{L}\right]^2$$

VI. CONCLUDING REMARKS AND RECOMMENDATIONS FOR FUTURE RESEARCH

The strain energy density failure criterion has been applied to several thermoelastic problems involving cracks and notches in domains with finite boundaries. Both thermal and mechanical loading are considered with a variety of different boundary conditions. The influence of notch tip sharpness on fracture path is investigated by determining the locations of $(dW/dV)_{min}$. This is achieved by calculating the stationary values of the strain energy density numerically and using an intra-element interpolation scheme in the finite element procedure. Numerical accuracy was established by comparing the numerical solution of a narrow notch in an uniform heat flow with the corresponding analytical solution of a line crack.

The expression for dW/dV contains not only the strain components but also a term, C_o, that depends on temperature and material properties. This term has been overlooked and can greatly influence the prediction of failure in solids with non-uniform temperature distributions. Examined are several examples where the predicted comparison of the paths for $C_o \neq 0$ and $C_o = 0$ are compared and discussed by varying the relative contribution of mechanical and thermal loading. In many cases, the neglect of C_o led to negative values of the strain energy density function which is a direct violation of the law of thermodynamics. In other instances, the discrepancies may be more subtle and go undetected.

The results of this investigation clearly show the merit of using a failure criterion based on the strain energy density function that depends on the energy level of the system in situations of non-uniform temperature state dictated by ΔT. The conventional criteria such as maximum stress, maximum strain, etc., cannot distinguish this difference and are therefore suspect on physical grounds because failure path is dependent on the energy level experienced by the solid.

By following the same procedure established in this work, the influence of permanent material damage can be included into the problem. This does not necessarily involve the incorporation of plasticity as it presents fundamental difficulties for describing loading and unloading in two- or three-dimensional stress fields. It is possible to develop non-linear damage accumulation theories based on the strain energy density theory [5]. Such an attempt is being made currently by researchers in the Institute of Fracture and Solid Mechanics at Lehigh University.

REFERENCES

[1] Sih, G. C., "A special theory of crack propagation: methods of analysis and solution of crack problems", Mechanics of Fracture I, edited by G. C. Sih, Noordhoff International Publishing, Leyden, pp. 21-45, 1973.

[2] Sih, G. C. and Matczyński, M., "Crack trajectories in non-isothermal environments predicted by strain energy density criterion", Journal of Theoretical and Applied Fracture Mechanics (to appear).

[3] Kipp, M. E. and Sih, G. C., "The strain energy density failure criterion applied to notched elastic solids", International Journal of Solids and Structures, 2, pp. 153-173, 1975.

[4] Sih, G. C., "Strain energy density and surface layer energy for blunted cracks or notches", Mechanics of Fracture V, edited by G. C. Sih, Noordhoff International Publishing, Leyden, pp. XIII-CX, 1978.

[5] Sih, G. C., "Experimental fracture mechanics: strain energy density criterion", Mechanics of Fracture VII, edited by G. C. Sih, Martinus Nijhoff, The Hague, pp. XVII-LVI, 1981.

[6] Fung, Y. C., Fundamentals of Solid Mechanics, Prentice-Hall, Englewood Cliffs, New Jersey, 1965.

[7] Boley, B. A. and Weiner, J. H., Theory of Thermal Stresses, John Wiley, 1960.

[8] Sokolnikoff, I. S., Mathematical Theory of Elasticity, McGraw-Hill, New York, 1956.

[9] Zienkiewicz, O. C., The Finite Element Method, Third Edition, McGraw-Hill, London, 1977.

[10] Hinton, E. and Owen, D. R. J., Finite Element Programming, Academic Press, London, 1977.

[11] Huebner, K. H., The Finite Element Method for Engineers, John Wiley, 1975.

[12] Bolton, R. C., Forthcoming Technical Report, Institute of Fracture and Solid Mechanics, Lehigh University.

[13] LEQT1B, International Mathematical and Statistical Libraries, Inc., Houston, Texas.

[14] Hilton, P. D., Gifford, L. N. and Lomacky, O., "Finite element fracture mechanics of two dimensional and axisymmetric elastic and elastic-plastic cracked structures", Naval Ship Research and Development Center Report No. 4493, 1975.

[15] Moyer, E. T., Jr., "Nonlinear aspects of fatigue crack propagation - a fracture mechanics approach", Unpublished Ph.D. Dissertation, Appendix D, Lehigh University, 1982.

[16] Sih, G. C., "Heat conduction in the infinite medium with lines of discontinuities", Journal of Heat Transfer, Vol. 87, p. 283, 1965.

VITA

Robert Charles Bolton, son of Dorothy M. and Franklin R. Bolton, was born July 5, 1955 in Reading, Pennsylvania. He graduated from Reading High School in June 1973. He attended the Massachusetts Institute of Technology from 1973 to 1976. He entered Lehigh University in September 1979 and received the Bachelor of Science degree in Mechanical Engineering with high honors in January 1982. He entered the Lehigh Graduate School in January 1982 in the Department of Mechanical Engineering receiving a one-year research Fellowship. He received the Elizabeth Major Nevius Award for outstanding fifth year students in October 1982. He married Lynne Uhl on December 30, 1982. He is a member of the ASME and Pi Tau Sigma.